

Hybrid Frequency Transmission for Upload Latency Minimization of IoT Devices in HSR Scenario Aided by Intelligent Reflecting Surfaces

Tianyou Li, Huawei Tong, *Student Member, IEEE*, Dapeng Li, *Member, IEEE*

Abstract—The explosively growing demand for Internet of Things (IoT) in high-speed railway (HSR) scenario has attracted a lot of attention amongst researchers. However, limited IoT device (IoTD) batteries and large information upload latency still remain critical impediments to practical service applications. In this paper, we consider a HSR wireless mobile communication system, where two intelligent reflecting surfaces (IRSs) are deployed to help solve the problems above. Considering the carrier aggregation method, the IRS needs to be optimized globally in hybrid frequency bands. Meanwhile, to ensure information security, the transmission to the mobile communication relay (MCR) on the train is covert to passengers in the carriage by IRS. This problem is challenging to handle since the variables are coupled with each other and some tricky constraints. We firstly transform the original sum-of-ratios problem into the more tractable parametric problem. Then, the block coordinate descent (BCD) algorithm is adopted to decouple the problem into two main sub-problems, and the downlink and uplink settings are alternatively optimized using low-complexity iterative algorithms. Finally, a heuristic algorithm to mitigate the Doppler spread is proposed to further improve the performance. Simulation results corroborate the performance improvement of the proposed algorithm.

Index Terms—Double intelligent reflecting surfaces, high-speed railway, internet of things, URLLC, optimization.

I. INTRODUCTION

RECENTLY, the investigation of high-speed railway (HSR) has attracted a lot of interest since an increasing number of people choose the convenient and economical way to travel to another place. With the rapid development of HSR, railway safety has attracted a great deal of attention [1, 2]. Real-time access to the information of railway system is one of the important issues to ensure railway safety. A large number of IoTDs are deployed on both sides of the tracks in order to obtain critical safety information such as road conditions and vehicle status in real time to ensure safe train operation [3, 4]. These IoTDs include temperature sensors, motion (accelerometer), smoke/fire detection sensors, real-time road condition monitoring, and so on [5, 6]. Undoubtedly, the HSR IoT system plays a very important role.

To meet the increasing capacity demands of railway IoT communication, the spectrum extension of 5G communications are envisaged at higher frequency bands with broader available spectrum, including frequency bands higher than 6 GHz, up to 300 GHz, since most of the spectrum sub-6 GHz

is already utilized currently. Some researchers proposed the heterogeneous network to solve the issue. Lower frequency bands, such as the existing cellular band of macro cells, are used to provide basic coverage while higher frequency bands in small cells are used to provide high-speed data transmission [7, 8]. In conclusion, high frequency system and low frequency systems in the railroad communication system will coexist for a long time, which has reached a consensus.

What's more, the HSR IoT systems still have many other issues that need to be overcome. With the development of railroad IoT, a large number of devices deployed along the trackside make the manual management of the battery very costly [9]. And the connection of wired devices makes it difficult to configure IoT systems. Hence, wireless power technology such as radio frequency energy harvesting may be employed to power and collect data from the low-power IoTDs [10, 11]. Although downlink transmission is dominated by passengers' communication, the train control information is more critical to the safe travel of the train and needs for priority reliable guarantee. Consequently, the information latency can have a significant impact on train safety. However, it can be large due to the information congestion caused by the large amount of information collected by IoTDs for uploading. Though in most cases the control data transmission from the IoTDs doesn't demand higher communication rates, with the development of railroad intelligent systems, the existing communication system can no longer meet the data rate needs of future railroad communication. For example, the cameras monitoring real-time road conditions need to upload high-definition images to the train, where complicated image compressed algorithms are often unavailable, making low transmission latency extremely difficult [12]. This latency may cause lag in train control operations and even cause serious accidents, especially in high speed scenarios.

Intelligent reflecting surface (IRS) techniques have been emerged as one of promising methods to solve this problem [13]. Many researchers have investigated the fundamental properties of IRS and its applications in various systems. Most recently, some initial efforts have been devoted to the HSR communication system aided by IRS. The applications of IRS in HSR communication systems were investigated in [14]. [15] proposed a deep reinforcement learning method, which makes real-time decision-making of beamforming truly viable in the dynamic HSR network. Moreover, the authors in [16] solved the sum rate maximization problem of multicell MIMO communication systems aided by IRS, which also applies to

This work was supported by grants from the National Natural Science Funds of China under Contract No. 62371246, 61701253 and 61801240. (Corresponding author: Dapeng Li email: dapengli@njupt.edu.cn)

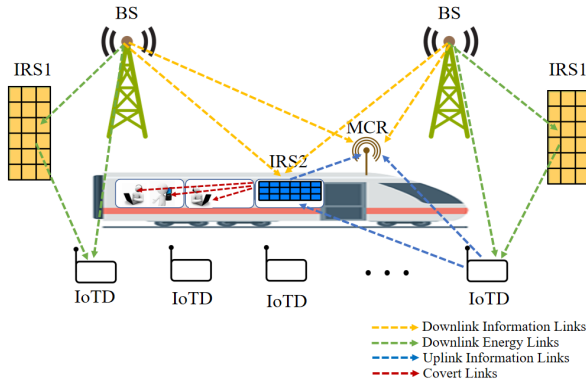


Fig. 1. Double-IRSs aided massive MIMO communication system in complex high-speed railway traveling environment. In each communication module, there are two IRSs and the base station with the IRS controller via the wireless backhaul link.

mobile scenarios. However, different from our work, it should be emphasized that all works above have been dedicated to maximizing the spectral efficiency of communication system. They all considered using IRS to optimize the communications from the BS to all users. [17, 18] considered channel estimation problem of IRS aided HSR system. They proposed low overhead channel estimation algorithms for high-speed scenarios. However, they didn't consider using IRS to improve performance of HSR system. [19] considered use IRS to suppress interference. They optimize the phase shifts to enhance the HSR network capacity against the interference. But they didn't consider the impact of IRS on information latency, nor did they consider collaboration between multiple frequency bands.

In this paper, we examine a WPCN to transfer power to the HSR IoT system aided by double IRS. We consider the cooperation in different frequency bands for performance improvement. In addition, typically the security of communication systems relies on upper-layer encryption, which encounters significant challenges in HSR IoT systems. This is mainly because all IoTDs are energy-limited, complicated secrecy protocols are often difficult to apply [20]. Physical layer security aided by IRS is a potential candidate for countering the above concern [21]. By carefully designing the phase shifts of the IRS, information leakage can be minimized and critical train data can be secured. The BS can not only transmit power to the high speed train, but also transmit information. Hence, the IRS2 can certainly be used to improve the performance of data transmission from users, which means hundreds of IRSs are required to be deployed along the trackside to meet long distances communication, although this is not the focus of this work. There has been a work that studied WPCN and IRS to maximize the sum-rate of IoT system [22] and it differs from our work in several points, which can be summarized as the main contributions in the following:

- We attempt to explore the assistance of multi IRSs in enhancing the WPCN in HSR IoT scenario. Inspired by [23, 24], we deploy double IRSs, with one deployed along the track and the other one as a transparent surface deployed on the train windows. The trackside surfaces are

used to assist in energy transfer, while the window surfaces assist in information transfer. This system paradigm facilitates the flexible deployment of trackside IoTDs and also enhances the battery life of IoTDs.

- Moreover, we investigate and formulate the weighted latency minimization of IoTDs data upload problem for the proposed MIMO system aided by double IRSs in HSR scenario. By introducing slack variables, we decouple the latency minimization problem into two sub-problems corresponding to the downlink energy transfer and uplink information upload phases. We reformulate the original problem into a more tractable form and propose to use the difference of convex algorithm to solve the energy beamforming matrix optimization in the downlink phase.
- Next, in the uplink phase, we consider the hybrid high and low frequency bands communication system, which can improve the reliability of the system. IRS2 reflects the incident signals of both high and low frequency bands, and achieves the local optimality in both frequency bands simultaneously. Then, the IRS2 increases the information transmission rate while communicating covertly to users in the carriage, ensuring that road and vehicle information will not be leaked, further guaranteeing train safety. We reformulate the original problem into the Semi-definite Relaxation (SDR) problem and relax the rank one constraint to solve it.
- Based on the optimized phase shifts by the proposed algorithm, they can be further adjusted by a low complexity heuristic algorithm to mitigate the Doppler spread, thus further improving performance. Finally, we provide a large number of numerical results to verify the effectiveness of our proposed hybrid transmission scheme and Doppler mitigation algorithm.

Organization: The rest of the paper is organized as follows. The system model and problem formulation are discussed in Section II. Our proposed algorithm is presented in Section III, IV and V. Results are described in Section VI and the conclusions are drawn in Section VII.

Notations: Bold lower and upper case letters denote vectors and matrices respectively. $\text{Tr}(\cdot)$ denotes the trace operator. $\mathbb{C}^{m \times n}$ denotes the space of complex matrices of dimensions given as in the superscripts m and n . For a general matrix \mathbf{A} , $\mathbf{A}_{(i,j)}$ denotes the (i,j) th element. The superscript $(\cdot)^T, (\cdot)^*, (\cdot)^H$ and $(\cdot)^{-1}$ stand for transpose, complex conjugate, Hermitian transpose and matrix inverse, respectively. \odot denotes the dot product. $\mathbb{E}\{\cdot\}$ stands for the statistical expectation. $x \sim U(a, b)$ represents a random variable following the uniform distribution between a and b . $x \sim \mathcal{CN}(0, \sigma^2)$ represents a random variable following the distribution of circularly symmetric complex Gaussian with zero mean and variance σ^2 . $\mathcal{O}(\cdot)$ denotes the standard big-O notation.

II. SYSTEM MODEL AND PROBLEM FORMULATION

In this section, we elaborate on the system model from both downlink energy transmission phase and uplink information transmission phase. As shown in Fig. 1, a wireless power communication HSR IoT system aided by double IRSs is

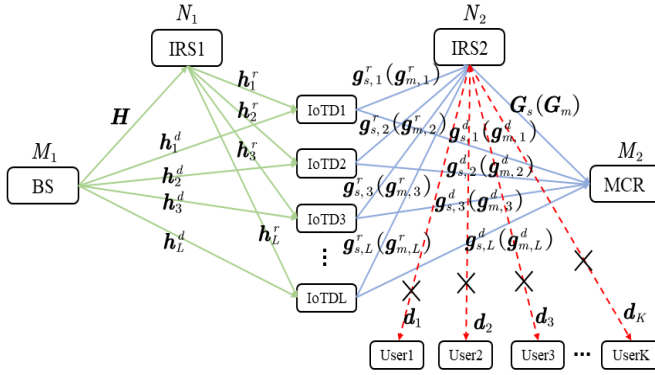


Fig. 2. The channel model shown in the figure is considered. In energy transmission phase, no matter what the frequency band of the signal can transmit energy, while in information transmission phase, the signal in the same frequency band is treated as noise.

considered in our work. For the sake of simplicity of problem formulation, we don't consider the BS/device handover problem when train travels across cells. Subsequently, a latency-minimization problem is formulated for our IRS-aided HSR IoT system, detailed as follows.

A. Energy Transmission Model

Considering a practical downlink energy transmission scenario consisting of one energy transmission BS, one IRS1, L single antenna IoTDs, which are deployed along the trackside to help trains operate safely. The set of IoTDs is defined as $\mathcal{L} = \{1, 2, \dots, L\}$. The number of antennas at the BS and passive reflecting elements at the IRS1 are denoted by M_1 and N_1 , respectively. The set of passive elements in IRS1 is defined as $\mathcal{N}_1 = \{1, 2, \dots, N_1\}$. Deploying wired energy transmission for each IoTD is extremely costly and unrealistic. For flexibility and scalability of deployment, in this phase, the BS needs to exploit wireless power transfer to L IoTDs. The IRS1 is deployed on the roadside to assist the energy transmission for all IoTDs. The downlink baseband channels from the BS to the IRS1, the IRS1 to the l th IoTD, the BS to the l th IoTD are denoted by $\mathbf{H} \in \mathbb{C}^{N_1 \times M_1}$, $\mathbf{h}_l^r \in \mathbb{C}^{1 \times N_1}$ and $\mathbf{h}_l^d \in \mathbb{C}^{1 \times M_1}$, respectively. By beneficially introducing the different phase shifts to the incident signals, the IRS1 can make them added constructively at all IoTDs to enhance the energy transfer efficiency. Let $\theta_{1,n_1} \in [0, 2\pi]$ be the phase shift introduced to the incident signals passing the n_1 th passive element by the IRS1. As for the amplitude reflection coefficient of the IRS1, we simply set it to 1 for all reflection elements, which has been proved to be optimal in [25]. In the following, a synchronous time-splitting protocol proposed in [26] is adopted in our work. Specifically, in the first βT ($0 < \beta < 1$) amount of time during each unit time, the BS transmits energy to all IoTDs. Then in the second $(1 - \beta)T$ amount of time, all IoTDs upload the information to the MCR for HSR operation safety. To facilitate analysis, the time block T is normalized to unit.

Generating multiple beams can help improve the fairness of energy harvesting when there are multiple IoTDs [27]. There-

fore, we assume that the fully-connected digital beamforming structure is deployed at the BS, so it can broadcast energy to all IoTDs through M_1 energy beams. The beam signal carrying energy can be presented as $\mathbf{x}_d = \sum_{i=1}^{M_1} \mathbf{w}_i s_i$, where $\mathbf{w}_i \in \mathbb{C}^{M_1 \times 1}$ denotes the i th downlink energy beam of \mathbf{W} and s_i denotes the energy carrying signal, which is assumed to be an independent identically distributed random variable with zero mean and unit variance. Therefore, the transmit power of the BS can be represented as $p_t = \mathbb{E}[\|\mathbf{x}_d\|^2] = \sum_{i=1}^{M_1} \|w_i\|^2$. Then, all IoTDs can receive the direct energy from the BS and the reflecting energy from the IRS1. Upon denoting the additive white Gaussian noise by $n \sim \mathcal{CN}(0, \sigma^2)$, the signal received at the l th IoTD is readily formulated as

$$y_{DL,l} = (\mathbf{h}_l^r \Phi_1 \mathbf{H} + \mathbf{h}_l^d) \mathbf{x}_d + n, \quad (1)$$

where $\Phi_1 = \text{diag}\{e^{j\theta_{1,1}}, \dots, e^{j\theta_{1,n_1}}, \dots, e^{j\theta_{1,N_1}}\}$ denotes the diagonal reflection-coefficients matrix. By defining the equivalent channel as $\bar{\mathbf{h}}_l \triangleq \mathbf{h}_l^r \Phi_1 \mathbf{H} + \mathbf{h}_l^d$, the energy received by the l th IoTD in the energy transmission phase can be expressed as

$$E_l = \xi \beta \mathbb{E}[|y_{DL,l}|^2] = \xi \beta \sum_{i=1}^{M_1} \bar{\mathbf{h}}_l \mathbf{w}_i \mathbf{w}_i^H \bar{\mathbf{h}}_l^H, \quad (2)$$

where $0 < \xi \leq 1$ is the energy transmission efficiency from the BS to IoTDs. By normalizing the uplink information transmission time, the transmitted power of the l th IoTD can be

$$p_l = \frac{E_l}{1 - \beta} = \frac{\xi \beta \sum_{i=1}^{M_1} \bar{\mathbf{h}}_l \mathbf{w}_i \mathbf{w}_i^H \bar{\mathbf{h}}_l^H}{1 - \beta}. \quad (3)$$

B. Information Transmission Model

Next, in the uplink information transmission phase, each IoTD needs to report information to the MCR, which is equipped M_2 antennas. Then the MCR transmits the information to the driver's compartment via wired transmission. Since the performance bottleneck of the second uplink phase lies in the wireless transmission part, we only focus on the hop from the IoTDs to the MCR. The IRS2 deployed on the train windows, which is equipped with N_2 passive elements, can be used to enhance the reflected signals from the IoTDs to the MCR. The set of passive elements in IRS2 is defined as $\mathcal{N}_2 = \{1, 2, \dots, N_2\}$. The users in the carriage act as legitimate eavesdroppers. Both the transmitter and receiver are aware of the presence of eavesdroppers and block the eavesdropper from receiving critical information. We denote the phase shifts of the n_2 th element of IRS2 as $\theta_{2,n_2} \in [0, 2\pi]$. Our proposed HSR IoT communication system can work in hybrid frequency band, so large bandwidth and high reliability can be guaranteed. Considering carrier aggregation technology, all IoTDs can choose to operate in both the sub-6 GHz with carrier frequency f_s and mmWave frequency band f_m to upload the information. Specifically, the report information can be represented as

$$\mathbf{x}_{\mathcal{F},l} = \sqrt{p_{\mathcal{F},l}} \mathbf{s}_{\mathcal{F},l}, \quad \mathcal{F} \in \{s, m\}, \quad (4)$$

where $s_{\mathcal{F},l}$ denotes the report information transmitted by the l th IoTD to the MCR, which satisfies $\mathbb{E}[s_{\mathcal{F}}^2] = 1$ and $\mathbb{E}[s_k s_l] =$

0, for $l \neq k$. And by defining the transmit power allocation factor $\gamma = [\gamma_1, \gamma_2, \dots, \gamma_L]$, we have $p_{s,l} = \gamma_l p_l$, $p_{m,l} = (1 - \gamma_l) p_l$. The uplink baseband channels from the IRS2 to the MCR, the l th IoTD to the IRS2, the l th IoTD to the MCR are denoted by $\mathbf{G}_{\mathcal{F}} \in \mathbb{C}^{M_2 \times N_2}$, $\mathbf{g}_{\mathcal{F},l}^r \in \mathbb{C}^{N_2 \times 1}$ and $\mathbf{g}_{\mathcal{F},l}^d \in \mathbb{C}^{M_2 \times 1}$, respectively. Covert communication baseband channel from the IRS2 to the k th user is denoted by $\mathbf{d}_{\mathcal{F},k} \in \mathbb{C}^{1 \times N_2}$.

The IRS2 deployed on the window is the transparent IRS whose copper backplane is removed [28]. It can work in transmissive type. By adjusting IRS structures such as element size, and metallic patch patterns, the incident signals can penetrate the elements. For sub-6 or mmWave band, the received signal at the MCR in the UL phase can be expressed as

$$\mathbf{y}_{\mathcal{F},UL} = \sum_{l=1}^L (\sqrt{p_{\mathcal{F},l}} (\mathbf{G}_{\mathcal{F}} \Phi_2 \mathbf{g}_{\mathcal{F},l}^r + \mathbf{g}_{\mathcal{F},l}^d) s_{\mathcal{F},l}) + \mathbf{n}_{\mathcal{F}}, \quad (5)$$

where $\mathbf{n}_{\mathcal{F}} = [n_{\mathcal{F},1}, n_{\mathcal{F},2}, \dots, n_{\mathcal{F},M_2}]$ for $n_{\mathcal{F},m_2} \sim \mathcal{CN}(0, \sigma_{\mathcal{F}}^2)$, $m_2 = 1, 2, \dots, M_2$ and $\Phi_2 = \text{diag}\{e^{j\theta_{2,1}}, \dots, e^{j\theta_{2,n_2}}, \dots, e^{j\theta_{2,N_2}}\}$. Then, at the receiver, the linear multi-user decoder technique is invoked to reduce the complexity. $\mathbf{F}_{\mathcal{F}} = [\mathbf{f}_{\mathcal{F},1}, \mathbf{f}_{\mathcal{F},2}, \dots, \mathbf{f}_{\mathcal{F},L}]$ denotes the multi-user decoder matrix. As for the l th IoTD, the recovered signal is presented as

$$\hat{s}_{\mathcal{F},l} = \mathbf{f}_{\mathcal{F},l}^H \left[\sum_{i=1}^L (\sqrt{p_{\mathcal{F},i}} (\mathbf{G}_{\mathcal{F}} \Phi_2 \mathbf{g}_{\mathcal{F},i}^r + \mathbf{g}_{\mathcal{F},i}^d) s_{\mathcal{F},i}) + \mathbf{n} \right]. \quad (6)$$

Then, the SINR of the l th IoTD's signal recovered is given by

$$\text{SINR}_{\mathcal{F},l} = \frac{p_{\mathcal{F},l} \mathbf{f}_{\mathcal{F},l}^H \bar{\mathbf{g}}_{\mathcal{F},l} \bar{\mathbf{g}}_{\mathcal{F},l}^H \mathbf{f}_{\mathcal{F},l}}{\mathbf{f}_{\mathcal{F},l}^H \left(\sum_{i=1, i \neq l}^L p_{\mathcal{F},i} \bar{\mathbf{g}}_{\mathcal{F},i} \bar{\mathbf{g}}_{\mathcal{F},i}^H + \sigma_{\mathcal{F}}^2 \mathbf{I} \right) \mathbf{f}_{\mathcal{F},l}}, \quad (7)$$

so the capacity of the channel for l th IoTD can be expressed as $C_{\mathcal{F},l} = (1 - \beta) B_{\mathcal{F}} \log_2 [1 + \text{SINR}_{\mathcal{F},l}]$, where $p_{s,l} + p_{m,l} = p_l$ and $\bar{\mathbf{g}}_{\mathcal{F},l} \triangleq (\mathbf{G}_{\mathcal{F}} \Phi_2 \mathbf{g}_{\mathcal{F},l}^r + \mathbf{g}_{\mathcal{F},l}^d)$ for $\mathcal{F} \in \{s, m\}$. At the same time, to ensure data security, uplink information transmission needs to be covert for K users in the carriage. The set of users is defined as $\mathcal{K} = \{1, 2, \dots, K\}$. Accordingly, the paths reflected by the IRS2 should be destructively superimposed at the user terminals, which can be presented as

$$\sum_{k=1}^K \sum_{l=1}^L |\mathbf{d}_{\mathcal{F},k} \Phi_2 \mathbf{g}_{\mathcal{F},l}^r|^2 = 0. \quad (8)$$

In our work, we assume that all CSI are perfectly known. Although some channel estimation schemes have been proposed, it's still challenging to perfectly estimate the channels in practical scenarios. Consequently the proposed algorithm can be deemed as the performance upper bound for the realistic scenarios. What's more, the high-speed train is characterized by periodically traveling along a fixed track, whose trajectory is highly predictable. In the practical application of the algorithm, the initial point of the proposed algorithm can be calculated in advance according to train's position as prior information, which can greatly reduce the number

of iterations. Upon defining the total volume of l th IoTD's upload information as v_l and the volume allocation factor $\alpha = [\alpha_1, \alpha_2, \dots, \alpha_L]^T$, from presented above, the information upload latency of the l th IoTD can be readily calculated by selecting the maximum value between those transmitted in the sub-6 GHz or the mmWave band, formulated as

$$D_l(\alpha, \beta, \mathbf{W}, \boldsymbol{\theta}_1, \gamma, \mathbf{F}, \boldsymbol{\theta}_2) = \max \left\{ \frac{\alpha_l v_l}{C_{s,l}}, \frac{(1 - \alpha_l) v_l}{C_{m,l}} \right\}. \quad (9)$$

C. Problem Formulation

In this work, we aim for minimizing sum weighted information upload latency of all IoTDs, by jointly optimizing variables β , α , \mathbf{W} , $\boldsymbol{\theta}_1$, \mathbf{p}_s , $\mathbf{F}_{\mathcal{F}}$ and $\boldsymbol{\theta}_2$. Specifically, upon defining the weight of the l th IoTD as ϖ_l , the weighted latency minimization problem is formulated as

$$\mathcal{P}0: \min_{\alpha, \beta, \mathbf{W}, \boldsymbol{\theta}_1, \gamma, \mathbf{F}, \boldsymbol{\theta}_2} \sum_{l=1}^L \varpi_l D_l \quad (10)$$

$$\text{s.t. } 0 < \beta < 1, \quad (10a)$$

$$0 \leq \alpha_l, \gamma_l \leq 1, \quad \forall l \in \mathcal{L}, \quad (10b)$$

$$0 \leq \theta_{1,n} < 2\pi, \quad \forall n \in \mathcal{N}_1, \quad (10c)$$

$$0 \leq \theta_{2,n} < 2\pi, \quad \forall n \in \mathcal{N}_2, \quad (10d)$$

$$\|\mathbf{W}\|_{\mathcal{F}}^2 \leq P_{\max}, \quad (10e)$$

$$\sum_{k=1}^K \sum_{l=1}^L |\mathbf{d}_{\mathcal{F},k} \Phi_2 \mathbf{g}_{\mathcal{F},l}^r|^2 = 0. \quad (10f)$$

(10a) and (10b) are allocation factor constraints. When $\alpha_l = 1$, it means that the channel conditions in the mmWave band are extremely poor and even blocked for the l th IoTD. At this time, the information should be all transmitted through the sub-6 band. When $\alpha_l = 0$ is the opposite; (10c) and (10d) specifies the range of the phase shifts of the passive elements deployed on the double IRSs. (10e) restrict the total transmit power at the BS side. Finally, (10f) represents the covert communication constraints for K users in the carriage.

The existing schemes are not applicable to solving the proposed problem due to the complex coupling effect of so many variables. It is a challenging problem to obtain a globally optimal solution directly. Consequently, we proposed a low complexity locally suboptimal solution to handle the proposed optimization problem, which will be described in detail in the next section.

III. OPTIMIZATION FOR DOWNLINK ENERGY TRANSMISSION

As mentioned above, owing to the coupling effect of many variables, the information upload weighted latency minimization problem cannot be solved directly. In this section, the BCD problem is proposed to handle $\mathcal{P}0$. Specifically, we firstly optimize the transmission volume allocation factor α . By reformulating the original problem into the more tractable form, we can decouple the problem into two subproblems—downlink energy optimization and uplink information optimization. Then, the formulated problem can be solved by alternately optimizing these subproblems. In this section, we

firstly focus our attention on the optimization of downlink energy transmission with uplink setting fixed.

For convenient analysis, we define $v_{s,l} \triangleq \alpha_l v_l$. Given $\beta, \mathbf{W}, \boldsymbol{\theta}_1, \gamma, \mathbf{F}, \boldsymbol{\theta}_2$, from (9), the information upload latency of the l th IoT can be reformulated as

$$D_l(\boldsymbol{\alpha}) = \begin{cases} \frac{v_l - v_{s,l}}{C_{m,l}}, & 0 \leq v_{s,l} \leq \frac{v_l C_{s,l}}{C_{s,l} + C_{m,l}}, \\ \frac{v_{s,l}}{C_{s,l}}, & \frac{v_l C_{s,l}}{C_{s,l} + C_{m,l}} < v_{s,l} \leq v_l. \end{cases} \quad (11)$$

It's obviously that $D_l(\boldsymbol{\alpha})$ decreases upon increasing $v_{s,l}$ in the range of $v_{s,l} \in \left[0, \frac{v_l C_{s,l}}{C_{s,l} + C_{m,l}}\right]$. And $D_l(\boldsymbol{\alpha})$ increases upon increasing $v_{s,l}$ in the range of $v_{s,l} \in \left(\frac{v_l C_{s,l}}{C_{s,l} + C_{m,l}}, v_l\right]$. Consequently, $D_l(\boldsymbol{\alpha})$ can achieve the minimum value when

$$v_{s,l}^* = \frac{v_l C_{s,l}}{C_{s,l} + C_{m,l}}. \quad (12)$$

Substituting (12) into (10), we can reformulate the objective function $\mathcal{P}0$ as

$$\mathcal{P}1: \min_{\beta, \mathbf{W}, \boldsymbol{\theta}_1, \gamma, \mathbf{F}, \boldsymbol{\theta}_2} \sum_{l=1}^L \frac{\varpi_l v_l}{C_{s,l} + C_{m,l}} \quad (13)$$

$$\text{s.t.} \quad (10a), (10c), (10e). \quad (13a)$$

It is easy to see that the problem $\mathcal{P}1$ is equivalent to the following problem.

$$\mathcal{P}1\text{-}E1: \min_{\beta, \mathbf{W}, \boldsymbol{\theta}_1, \gamma, \mathbf{F}, \boldsymbol{\theta}_2, \boldsymbol{\eta}} \sum_{l=1}^L \eta_l \quad (14)$$

$$\text{s.t.} \quad \frac{\varpi_l v_l}{C_{s,l} + C_{m,l}} \leq \eta_l, \quad \forall l \in \mathcal{L}, \quad (14a)$$

$$(10a), (10c), (10e). \quad (14b)$$

We construct the Lagrangian of $\mathcal{P}1\text{-}E1$ which is formulated as

$$\mathcal{L}(\mathcal{C}_{\mathcal{F}}, \boldsymbol{\lambda}, \boldsymbol{\eta}) = \sum_{l=1}^L \eta_l + \sum_{l=1}^L \lambda_l [\varpi_l v_l - \eta_l (C_{s,l} + C_{m,l})]. \quad (15)$$

If $(\mathcal{C}_{\mathcal{F}}^*, \boldsymbol{\eta}^*)$ is the solution of the problem $\mathcal{P}1\text{-}E1$, there must exist $\boldsymbol{\lambda}^*$ such that the following Karush-Kuhn-Tucker (KKT) conditions are satisfied

$$-\lambda_l^* \eta_l^* (\nabla C_{s,l}^* + \nabla C_{m,l}^*) = 0, \quad l \in \mathcal{L}, \quad (16)$$

$$\frac{\partial \mathcal{L}}{\partial \eta_l} = 1 - \lambda_l^* (C_{s,l}^* + C_{m,l}^*) = 0, \quad l \in \mathcal{L}, \quad (17)$$

$$\lambda_l^* [\varpi_l v_l - \eta_l^* (C_{s,l}^* + C_{m,l}^*)] = 0, \quad l \in \mathcal{L}, \quad (18)$$

$$\lambda_l^* \geq 0, \quad l \in \mathcal{L}, \quad (19)$$

$$\varpi_l v_l - \eta_l^* (C_{s,l}^* + C_{m,l}^*) \leq 0 \quad l \in \mathcal{L}. \quad (20)$$

From (17) and (18), we can easily obtain

$$\lambda_l^* = \frac{1}{C_{s,l}^* + C_{m,l}^*}, \quad \eta_l^* = \frac{\varpi_l v_l}{C_{s,l}^* + C_{m,l}^*}, \quad (21)$$

where $\mathcal{C}_{\mathcal{F}}^* \triangleq \mathcal{C}_{\mathcal{F}}(\beta^*, \mathbf{W}^*, \boldsymbol{\theta}_1^*, \gamma^*, \mathbf{F}^*, \boldsymbol{\theta}_2^*)$ for $\mathcal{F} \in \{s, m\}$. Then, with $\boldsymbol{\lambda}$ and $\boldsymbol{\eta}$ are initialized and fixed, we can reformulate the $\mathcal{P}1\text{-}E1$ as the following equivalent problem

$$\mathcal{P}1\text{-}E2: \min_{\beta, \mathbf{W}, \boldsymbol{\theta}_1, \gamma, \mathbf{F}, \boldsymbol{\theta}_2} \sum_{l=1}^L \lambda_l [\varpi_l v_l - \eta_l (C_{s,l} + C_{m,l})] \quad (22)$$

$$\text{s.t.} \quad (10a), (10c), (10e). \quad (22a)$$

By now, we have transformed the sum-of-ratios problem into the more tractable parametric problem. Next, we will optimize the downlink energy transmission setting.

A. Optimization of β

Given $\boldsymbol{\alpha}, \mathbf{W}, \boldsymbol{\theta}_1, \gamma, \mathbf{F}, \boldsymbol{\theta}_2$, problem $\mathcal{P}1\text{-}E2$ for optimizing time allocation variable β can be transformed as

$$\mathcal{P}2: \max_{\beta} \sum_{l=1}^L \lambda_l \eta_l (C_{s,l} + C_{m,l}) \quad (23)$$

$$\text{s.t.} \quad 0 < \beta < 1. \quad (23a)$$

Defining $a_{s,l} = \xi \sum_{i=1}^{M_1} \gamma_l \bar{\mathbf{h}}_l \mathbf{w}_i \mathbf{w}_i^H \bar{\mathbf{h}}_l^H \mathbf{f}_{s,l}^H \bar{\mathbf{g}}_{s,l} \bar{\mathbf{g}}_{s,l}^H \mathbf{f}_{s,l}$, $b_{s,l} = \xi \sum_{j=1, j \neq l}^L \sum_{i=1}^{M_1} \gamma_j \bar{\mathbf{h}}_j \mathbf{w}_i \mathbf{w}_i^H \bar{\mathbf{h}}_j^H \mathbf{f}_{s,l}^H \bar{\mathbf{g}}_{s,j} \bar{\mathbf{g}}_{s,j}^H \mathbf{f}_{s,l}$, $c_{s,l} = \sigma_s^2 \mathbf{f}_{s,l}^H \mathbf{f}_{s,l}$, $a_{m,l} = \xi \sum_{i=1}^{M_1} (1 - \gamma_l) \bar{\mathbf{h}}_l \mathbf{w}_i \mathbf{w}_i^H \bar{\mathbf{h}}_l^H \mathbf{f}_{m,l}^H \bar{\mathbf{g}}_{m,l} \bar{\mathbf{g}}_{m,l}^H \mathbf{f}_{m,l}$, $b_{m,l} = \xi \sum_{j=1, j \neq l}^L \sum_{i=1}^{M_1} (1 - \gamma_j) \bar{\mathbf{h}}_j \mathbf{w}_i \mathbf{w}_i^H \bar{\mathbf{h}}_j^H \mathbf{f}_{m,l}^H \bar{\mathbf{g}}_{m,j} \bar{\mathbf{g}}_{m,j}^H \mathbf{f}_{m,l}$ and $c_{m,l} = \sigma_m^2 \mathbf{f}_{m,l}^H \mathbf{f}_{m,l}$, respectively. The objective problem $\mathcal{P}2$ can be reformulated as

$$\mathcal{P}2\text{-}E1: \max_{\beta} \sum_{l=1}^L \sum_{\mathcal{F} \in \{s, m\}} f_{\mathcal{F},l}(\beta), \quad (24)$$

where $f_{\mathcal{F},l}(\beta) = \lambda_l \eta_l B_{\mathcal{F}} (1 - \beta) \log_2 \left(1 + \frac{\beta a_{\mathcal{F},l}}{(b_{\mathcal{F},l} - c_{\mathcal{F},l})\beta + c_{\mathcal{F},l}}\right)$ with $0 < \beta < 1$. $\mathcal{P}2\text{-}E1$ is a convex optimization problem with respect to β . The second order function of $\mathcal{P}2\text{-}E$ is strictly less than 0 in $0 < \beta < 1$. Hence, a low complexity search method based on bisection is adopted to search the optimal β^* which satisfies $\frac{\partial (f_{\mathcal{F},l})}{\partial \beta} = 0$.

B. Joint Optimization of \mathbf{W} and $\boldsymbol{\theta}_1$

Given $\boldsymbol{\alpha}, \beta, \gamma, \mathbf{F}, \boldsymbol{\theta}_2$, problem $\mathcal{P}1\text{-}E2$ can be given as

$$\mathcal{P}3: \max_{\mathbf{W}, \boldsymbol{\theta}_1} \sum_{l=1}^L \sum_{\mathcal{F} \in \{s, m\}} \lambda_l \eta_l C_{\mathcal{F},l} \quad (25)$$

$$\text{s.t.} \quad (10c), (10e). \quad (25a)$$

From [29], the original problem can be reformulated as

$$\mathcal{P}3\text{-}E1: \min_{\mathbf{W}, \boldsymbol{\theta}_1} \sum_{l=1}^L \sum_{\mathcal{F} \in \{s, m\}} \left(\Gamma_{\mathcal{F},l} e_{\mathcal{F},l}(\mathbf{W}, \boldsymbol{\theta}_1) - \lambda_l \eta_l B_{\mathcal{F}} - \lambda_l \eta_l B_{\mathcal{F}} \log_2 \left(\frac{\Gamma_{\mathcal{F},l}}{\lambda_l \eta_l B_{\mathcal{F}}} \right) \right) \quad (26)$$

$$\text{s.t.} \quad (10c), (10e) \quad (26a)$$

where $\Gamma_{\mathcal{F},l}$ is the newly introduced auxiliary variable and $e_{\mathcal{F},l}$ for $\mathcal{F} \in \{s, m\}$ represents the MSE of the l -th IoTD in sub-6 GHz or mmWave band, which is given by

$$\begin{aligned} e_{\mathcal{F},l} &\triangleq \mathbb{E} \left[(\hat{s}_{\mathcal{F},l} - s_{\mathcal{F},l}) (\hat{s}_{\mathcal{F},l} - s_{\mathcal{F},l})^H \right] \\ &= \left(\sqrt{p_{\mathcal{F},l}} \mathbf{f}_{\mathcal{F},l}^H \bar{\mathbf{g}}_{\mathcal{F},l} - 1 \right) \left(\sqrt{p_{\mathcal{F},l}} \mathbf{f}_{\mathcal{F},l}^H \bar{\mathbf{g}}_{\mathcal{F},l} - 1 \right)^H \\ &\quad + \sum_{i \neq l}^L p_{\mathcal{F},i} \mathbf{f}_{\mathcal{F},i}^H \bar{\mathbf{g}}_{\mathcal{F},i} \bar{\mathbf{g}}_{\mathcal{F},i}^H \mathbf{f}_{\mathcal{F},l} + \sigma_{\mathcal{F}}^2 \mathbf{f}_{\mathcal{F},l}^H \mathbf{f}_{\mathcal{F},l}. \end{aligned} \quad (27)$$

1) *Optimization of $\Gamma_{\mathcal{F},l}$* : With given \mathbf{W}, θ_1 , we take the first order derivative of $\mathcal{P}3$ -E1 with respect to $\Gamma_{\mathcal{F},l}$ and set it equal to zero. The optimal $\Gamma_{\mathcal{F},l}^*$ can be achieved by

$$\Gamma_{\mathcal{F},l} = \lambda_l \eta_l B_{\mathcal{F}} e_{\mathcal{F},l}^{-1}. \quad (28)$$

2) *Optimization of \mathbf{W}* : With given $\Gamma_{\mathcal{F},l}, \theta_1$, $\mathcal{P}3$ -E can be rewritten as

$$\mathcal{P}3\text{-E2} : \min_{\mathbf{W}} \sum_{l=1}^L \sum_{\mathcal{F} \in \{s, m\}} \Gamma_{\mathcal{F},l} e_{\mathcal{F},l}(\mathbf{W}) \quad (29)$$

$$\text{s.t. } \|\mathbf{W}\|_F^2 \leq P_{\max}. \quad (29a)$$

The objective function $\mathcal{P}3$ -E2 is nonconvex because of the nonconvex $e_{\mathcal{F},l}(\mathbf{W})$. By defining $q_{\mathcal{F},l,i} \triangleq \mathbf{f}_{\mathcal{F},l}^H \bar{\mathbf{g}}_{\mathcal{F},i}$ and substituting (3) into (27), $e_{\mathcal{F},l}$ can be reformulated as

$$\begin{aligned} e_{\mathcal{F},l} &= \sum_{i=1}^L \bar{\gamma}_{\mathcal{F},i} q_{\mathcal{F},l,i} q_{\mathcal{F},l,i}^H \|\bar{\mathbf{h}}_i \mathbf{W}\|^2 + \sigma_{\mathcal{F}}^2 \mathbf{f}_{\mathcal{F},l}^H \mathbf{f}_{\mathcal{F},l} \\ &\quad - (q_{\mathcal{F},l,l} + q_{\mathcal{F},l,l}^H) \sqrt{\bar{\gamma}_{\mathcal{F},l}} \|\bar{\mathbf{h}}_l \mathbf{W}\| + 1, \end{aligned} \quad (30)$$

where $\bar{\gamma}_{s,i} \triangleq \frac{\gamma_i \xi \beta}{1-\beta}$ and $\bar{\gamma}_{m,i} \triangleq \frac{(1-\gamma_i) \xi \beta}{1-\beta}$. By substituting (30) into (29) and omitting the constant, we can reformulate the problem $\mathcal{P}3$ -E2 as following:

$$\mathcal{P}3\text{-E3} : \min_{\mathbf{W}} f(\mathbf{W}) = g(\mathbf{W}) - h(\mathbf{W}) \quad (31)$$

$$\text{s.t. } \|\mathbf{W}\|_F^2 \leq P_{\max}, \quad (31a)$$

where

$$g(\mathbf{W}) = \sum_{l=1}^L \sum_{\mathcal{F} \in \{s, m\}} \sum_{i=1}^L \Gamma_{\mathcal{F},l} \bar{\gamma}_{\mathcal{F},i} q_{\mathcal{F},l,i} q_{\mathcal{F},l,i}^H \|\bar{\mathbf{h}}_i \mathbf{W}\|^2, \quad (32)$$

$$h(\mathbf{W}) = \sum_{l=1}^L \sum_{\mathcal{F} \in \{s, m\}} \Gamma_{\mathcal{F},l} 2 \text{Re}(q_{\mathcal{F},l,l}) \sqrt{\bar{\gamma}_{\mathcal{F},l}} \|\bar{\mathbf{h}}_l \mathbf{W}\|. \quad (33)$$

$g(\mathbf{W})$ and $h(\mathbf{W})$ are both convex functions with respect to \mathbf{W} . To calculate the optimal \mathbf{W} under the power constraint, we use the Difference of Convex algorithm (DCA) [30] to handle this non-convex problem. Based on the local optimality conditions and duality in difference of convex programming, the overarching method of the algorithm is to create two sequences of variables, $\mathbf{W}^t, \mathbf{V}^t$ so that \mathbf{W} converges to a local optimum of the primal problem, \mathbf{W}^* , and \mathbf{V} converges to the local optimum of the dual problem, \mathbf{V}^* . By calculating the gradient of $h(\mathbf{W})$ with respect to \mathbf{W} , we can obtain \mathbf{V}^t , which is given as follows:

$$\frac{\partial h}{\partial \mathbf{W}} = \sum_{l=1}^L \sum_{\mathcal{F} \in \{s, m\}} \Gamma_{\mathcal{F},l} \text{Re}(q_{\mathcal{F},l,l}) \sqrt{\bar{\gamma}_{\mathcal{F},l}} \frac{\mathbf{W}^H \bar{\mathbf{h}}_l^H \bar{\mathbf{h}}_l}{\|\bar{\mathbf{h}}_l \mathbf{W}\|}. \quad (34)$$

Algorithm 1 DCA for the Energy Matrix \mathbf{W}

Input: max number of iterations $T_{DCA, \max}$, convergence error ϵ , initial value of \mathbf{W}

Output: optimal \mathbf{W}^*

1: Initial $t = 0$ and $\mathbf{W}^t = \mathbf{W}$.

2: **Repeat**

 Calculate \mathbf{V}^t according to (34),

 Optimize the convex problem (35) and $t = t + 1$.

3: **Until** $\frac{\|\mathbf{W}^{t+1} - \mathbf{W}^t\|_F^2}{\|\mathbf{W}^t\|_F^2} \leq \epsilon$ or $T_{DCA, \max} = t$.

4: Output $\mathbf{W}^* = \mathbf{W}^t$.

Next, we can update the \mathbf{W}^{t+1} by optimizing the convex problem

$$\arg \min \{g(\mathbf{W}) - [h(\mathbf{W}^t) + \langle \mathbf{W} - \mathbf{W}^t, \mathbf{V}^t \rangle]\} \quad (35)$$

$$\text{s.t. } \|\mathbf{W}\|_F^2 \leq P_{\max}. \quad (35a)$$

where $\langle \mathbf{X}, \mathbf{Y} \rangle$ denotes the inner product of \mathbf{X} and \mathbf{Y} . The DCA for solving Problem $\mathcal{P}3$ -E2 is concluded in Algorithm 1. The complexity of calculating \mathbf{V}^t in Algorithm 1 is $\mathcal{O}(LM_1^2)$. And the complexity of optimizing the convex problem (35) is $\mathcal{O}\left(\frac{M_1^4 \sqrt{\log(M_1^2)}}{\epsilon_{DCA}^2}\right)$, where ϵ_{DCA}^2 is the target precision of convex optimization. The overall complexity of Algorithm 1 is $\mathcal{O}\left(t_1 \left(\frac{M_1^4 \sqrt{\log(M_1^2)}}{\epsilon_{DCA}^2} + LM_1^2\right)\right)$, where t_1 denotes the total number of iterations.

3) *Optimization of θ_1* : With given Γ, \mathbf{W} , the objective has changed to optimize the phase shifts of IRS1 to improve the efficiency of energy transmit rewritten as follows:

$$\mathcal{P}4 : \min_{\mathbf{W}} \sum_{l=1}^L \sum_{\mathcal{F} \in \{s, m\}} \Gamma_{\mathcal{F},l} e_{\mathcal{F},l}(\theta_1) \quad (36)$$

$$\text{s.t. } 0 \leq \theta_{1,n} < 2\pi, \quad n \in \mathcal{N}_1. \quad (36a)$$

which is a non-convex problem due to the constraint (36a). The similar problem has been investigated in the previous work [22]. Therefore, we used the algorithm in [22] called *SCA for the DL Phase Shift Optimization* to deal with this problem. The total complexity of the algorithm is $\mathcal{O}(t_2 L^2 N_1^2)$, where t_2 denotes the total number of iterations that guarantees the convergence. By updating the variables ϕ_1^{t+1} in the $(t+1)$ th iteration alternately, the convergence can be achieved. The details of this algorithm are omitted for brevity, which can be found in [22].

IV. OPTIMIZATION FOR TRANSMISSION OF UPLINK INFORMATION

In this section, with downlink setting optimized and fixed, let us explore how to optimize the uplink information transmission phase.

A. Optimization of γ

Given \mathbf{W}, θ_1 and fixed, the transmitting power of each IoTD is determined. The weighted information upload latency minimization problem optimized for γ can be transformed into a power allocation problem in the sub-6 GHz and mmWave

bands for each IoT. We can obtain the optimal power allocation factor γ_l by optimizing the following problem

$$\begin{aligned} \mathcal{P5} : \max_{\gamma} & \sum_{\mathcal{F}}^{F \in \{s,m\}} B_{\mathcal{F}} \log_2(1 + \text{SINR}_{\mathcal{F},l}) \quad (37) \\ \text{s.t.} & 0 \leq \gamma_l \leq 1, \quad l \in \mathcal{L}. \quad (37a) \end{aligned}$$

Considering that the interference in the same band can vary with the γ , we can optimal γ_l device by device and the decreasing objective function value of Problem $\mathcal{P1}$ is still guaranteed.

By deriving the optimal solution for γ_l by setting the first-order derivative of $\mathcal{P5}$ with respect to γ_l to zero, we can obtain

$$\begin{aligned} B_s \frac{q_{s,l,l}}{\ln 2 \left(\sum_i^L \gamma_i p_i q_{s,l,i} + \sigma_s^2 \mathbf{f}_{\mathcal{F},l}^H \mathbf{f}_{\mathcal{F},l} \right)} \\ - B_m \frac{q_{m,l,l}}{\ln 2 \left(\sum_i^L (1 - \gamma_i) p_i q_{m,l,i} + \sigma_m^2 \mathbf{f}_{\mathcal{F},l}^H \mathbf{f}_{\mathcal{F},l} \right)} = 0. \quad (38) \end{aligned}$$

Similar as the optimization of β in Section III. B, we adopt the search method based on bisection to find the optimal γ_l^* which satisfies (38).

B. Joint Optimization of \mathbf{F} and θ_2

Similar as $\mathcal{P3-E1}$, the rate maximization problem can be transformed into the MSE minimization problem presented as

$$\begin{aligned} \mathcal{P6} : \min_{\mathbf{F}, \theta_2} & \sum_{l=1}^L \sum_{\mathcal{F} \in \{s,m\}} (\Gamma_{\mathcal{F},l} e_{\mathcal{F},l}(\mathbf{F}, \theta_2) - \lambda_l \eta_l B_{\mathcal{F}} \quad (39) \\ & - \lambda_l \eta_l B_{\mathcal{F}} \log_2(\Gamma_{\mathcal{F},l} / (\lambda_l \eta_l B_{\mathcal{F}})) \\ \text{s.t.} & (10d), (10f). \quad (39a) \end{aligned}$$

1) *Optimization of \mathbf{F}* : With $\Gamma_{\mathcal{F},l}$ and θ_2 fixed, $\mathcal{P6}$ is a concave function of \mathbf{F} . we can derive the optimal solution by setting the first-order derivative of $\mathcal{P6}$ with respect to \mathbf{F} to zero

$$\mathbf{f}_{\mathcal{F},l}^* = \left(\sum_{i=1}^L p_{\mathcal{F},i} \bar{\mathbf{g}}_{\mathcal{F},i} \bar{\mathbf{g}}_{\mathcal{F},i}^H + \sigma_{\mathcal{F}}^2 \mathbf{I}_{M_2} \right)^{-1} (\sqrt{p_{\mathcal{F},l}} \bar{\mathbf{g}}_{\mathcal{F},l}). \quad (40)$$

2) *Optimization of θ_2* : With other variables all fixed and constants omitted, we can get the following equation

$$\begin{aligned} & \sum_{l=1}^L \sum_{i=1}^L \Gamma_{\mathcal{F},l} p_{\mathcal{F},i} \mathbf{f}_{\mathcal{F},l}^H \bar{\mathbf{g}}_{\mathcal{F},i} \bar{\mathbf{g}}_{\mathcal{F},i}^H \mathbf{f}_{\mathcal{F},l} \\ = & \sum_{l=1}^L \sum_{i=1}^L \left(\Gamma_{\mathcal{F},l} p_{\mathcal{F},i} \mathbf{f}_{\mathcal{F},l}^H \mathbf{G}_{\mathcal{F}} \Phi_2 \mathbf{g}_{\mathcal{F},i}^r \mathbf{g}_{\mathcal{F},i}^r{}^H \Phi_2^H \mathbf{G}_{\mathcal{F}}^H \mathbf{f}_{\mathcal{F},l} \right. \\ & + \Gamma_{\mathcal{F},l} p_{\mathcal{F},i} \mathbf{f}_{\mathcal{F},l}^H \mathbf{g}_{\mathcal{F},i}^d \mathbf{g}_{\mathcal{F},i}^r{}^H \Phi_2^H \mathbf{G}_{\mathcal{F}}^H \mathbf{f}_{\mathcal{F},l} \\ & \left. + \Gamma_{\mathcal{F},l} p_{\mathcal{F},i} \mathbf{f}_{\mathcal{F},l}^H \mathbf{G}_{\mathcal{F}} \Phi_2 \mathbf{g}_{\mathcal{F},i}^r \mathbf{g}_{\mathcal{F},i}^d{}^H \mathbf{f}_{\mathcal{F},l} \right), \quad (41) \end{aligned}$$

$$\begin{aligned} & \sum_{l=1}^L \Gamma_{\mathcal{F},l} \sqrt{p_{\mathcal{F},l}} \bar{\mathbf{g}}_{\mathcal{F},l}^H \mathbf{f}_{\mathcal{F},l} \\ = & \sum_{l=1}^L \left(\Gamma_{\mathcal{F},l} \sqrt{p_{\mathcal{F},l}} \mathbf{g}_{\mathcal{F},l}^d{}^H \mathbf{f}_{\mathcal{F},l} + \Gamma_{\mathcal{F},l} \sqrt{p_{\mathcal{F},l}} \mathbf{g}_{\mathcal{F},l}^r{}^H \Phi_2^H \mathbf{G}_{\mathcal{F}}^H \mathbf{f}_{\mathcal{F},l} \right), \quad (42) \end{aligned}$$

For convenient analysis, We define all variables that are independent of θ_2 in the following form

$$\mathbf{A}_{\mathcal{F}} \triangleq \sum_{l=1}^L \Gamma_{\mathcal{F},l} \mathbf{G}_{\mathcal{F}}^H \mathbf{f}_{\mathcal{F},l} \mathbf{f}_{\mathcal{F},l}^H \mathbf{G}_{\mathcal{F}}, \quad (43)$$

$$\mathbf{B}_{\mathcal{F}} \triangleq \sum_{i=1}^L p_{\mathcal{F},i} \mathbf{g}_{\mathcal{F},i}^r \mathbf{g}_{\mathcal{F},i}^r{}^H, \quad (44)$$

$$\mathbf{C}_{\mathcal{F}} \triangleq \sum_{l=1}^L \sum_{i=1}^L \Gamma_{\mathcal{F},l} p_{\mathcal{F},i} \mathbf{g}_{\mathcal{F},i}^r \mathbf{g}_{\mathcal{F},i}^d{}^H \mathbf{f}_{\mathcal{F},l} \mathbf{f}_{\mathcal{F},l}^H \mathbf{G}_{\mathcal{F}}, \quad (45)$$

$$\mathbf{D}_{\mathcal{F}} \triangleq \sum_{l=1}^L \Gamma_{\mathcal{F},l} \sqrt{p_{\mathcal{F},l}} \mathbf{g}_{\mathcal{F},l}^r \mathbf{f}_{\mathcal{F},l}^H \mathbf{G}_{\mathcal{F}}. \quad (46)$$

Substituting (44)~(46) into (27) and omitting all constant, we can obtain

$$\begin{aligned} \sum_{l=1}^L \Gamma_{\mathcal{F},l} e_{\mathcal{F},l} = & \text{Tr}(\Phi_2^H \mathbf{A}_{\mathcal{F}} \Phi_2 \mathbf{B}_{\mathcal{F}}) + \text{Tr}(\Phi_2^H (\mathbf{C}_{\mathcal{F}} - \mathbf{D}_{\mathcal{F}})^H) \\ & + \text{Tr}(\Phi_2 (\mathbf{C}_{\mathcal{F}} - \mathbf{D}_{\mathcal{F}})). \quad (47) \end{aligned}$$

Therefore, by defining $\mathbf{E} = \sum_{\mathcal{F}}^{s,m} \mathbf{C}_{\mathcal{F}} - \sum_{\mathcal{F}}^{s,m} \mathbf{D}_{\mathcal{F}}$, we substitute (47) into $\mathcal{P3-E}$. After omitting the constant terms, the objective function can be rewritten as

$$\begin{aligned} \mathcal{P6-E1} : \min_{\theta_2} & \text{Tr}(\Phi_2^H \mathbf{A}_s \Phi_2 \mathbf{B}_s) + \text{Tr}(\Phi_2^H \mathbf{A}_m \Phi_2 \mathbf{B}_m) \\ & + \text{Tr}(\Phi_2^H \mathbf{E}^H) + \text{Tr}(\Phi_2 \mathbf{E}) \quad (48) \\ \text{s.t.} & (10d), (10f). \quad (48a) \end{aligned}$$

Upon defining $\phi_2 \triangleq [e^{j\theta_{2,1}}, e^{j\theta_{2,2}}, \dots, e^{j\theta_{2,N_2}}]^T$, and $\mathbf{e} = [\mathbf{E}_{(1,1)}, \mathbf{E}_{(2,2)}, \dots, \mathbf{E}_{(N_2, N_2)}]$, according to the properties of matrix transformation, from [31], we can get

$$\text{Tr}(\Phi_2^H \mathbf{A}_{\mathcal{F}} \Phi_2 \mathbf{B}_{\mathcal{F}}) = \phi_2^H (\mathbf{A}_{\mathcal{F}} \odot \mathbf{B}_{\mathcal{F}}^T) \phi_2, \quad (49)$$

$$\text{Tr}(\Phi_2 \mathbf{E}) = \mathbf{e} \phi_2, \quad \text{Tr}(\Phi_2^H \mathbf{E}^H) = \phi_2^H \mathbf{e}^H. \quad (50)$$

Accordingly, the objective function can be reformulated as

$$\begin{aligned} \mathcal{P6-E2} : \min_{\theta_2} & f(\theta_2) = \phi_2^H \Xi \phi_2 + \mathbf{e} \phi_2 + \phi_2^H \mathbf{e}^H \quad (51) \\ \text{s.t.} & (10d), (10f), \quad (51a) \end{aligned}$$

where $\Xi \triangleq \mathbf{A}_s \odot \mathbf{B}_s^T + \mathbf{A}_m \odot \mathbf{B}_m^T$. Next, by introducing an auxiliary variable t which satisfies $t^2 = 1$, we can get the optimization objective as follows

$$\mathcal{P6-E3} : \min_{\theta_2} \bar{\phi}_2^H \Lambda \bar{\phi}_2 \quad (52)$$

$$\text{s.t.} (10d), (10f), \quad (52a)$$

where we define

$$\Lambda \triangleq \begin{bmatrix} \Xi & \mathbf{e}^H \\ \mathbf{e} & 0 \end{bmatrix}, \quad \bar{\phi}_2 \triangleq \begin{bmatrix} \phi_2 \\ t \end{bmatrix}. \quad (53)$$

The covert communication constraints will be analysed in the following. From (10f), we can get

$$\mathbf{d}_{\mathcal{F},k} \Phi_2 \mathbf{g}_{\mathcal{F},l}^r \mathbf{g}_{\mathcal{F},l}^r{}^H \Phi_2^H \mathbf{d}_{\mathcal{F},k}^H = 0, \quad \mathcal{F} \in \{s, m\}, l \in \mathcal{L}, k \in \mathcal{K}. \quad (54)$$

Algorithm 2 SDR Algorithm to Optimize θ_2

Input: $d_{\mathcal{F},k}, k = 1, \dots, K, \mathbf{g}_{\mathcal{F},l}^r, l = 1, \dots, L, \Xi, \mathbf{e}, N_{rand}$

Output: optimal $\bar{\phi}_2^*$

- 1: Initial Λ and $\tilde{\Delta}$ according to (53) and (57).
 - 2: Optimize the problem $\mathcal{P}6-E4$ to get the optimal Ω^* .
 - 3: Make the eigenvalue decomposition of $\Omega^* = \mathbf{U}\Sigma\mathbf{U}^H$.
 - 4: Generate N_{rand} realizations of $\bar{\phi}_2 = \mathbf{U}\Sigma^{\frac{1}{2}}\mathbf{r}$, where $\mathbf{r} \sim \mathcal{CN}(0, \mathbf{I}_{N_2+1})$.
 - 5: Select the optimal $\bar{\phi}_2^*$ by maximizing the $\bar{\phi}_2\Lambda\bar{\phi}_2^H$.
 - 6: Normalize the $\bar{\phi}_2^*$ as (58).
-

Then, we reformulate (54) as

$$\begin{aligned}
 & d_{\mathcal{F},k}\Phi_2\mathbf{g}_{\mathcal{F},l}^r\mathbf{g}_{\mathcal{F},l}^{rH}\Phi_2^H d_{\mathcal{F},k}^H \\
 \stackrel{(a_1)}{=} & \text{Tr}\left(\Phi_2^H d_{\mathcal{F},k}^H d_{\mathcal{F},k} \Phi_2 \mathbf{g}_{\mathcal{F},l}^r \mathbf{g}_{\mathcal{F},l}^{rH}\right) \\
 \stackrel{(a_2)}{=} & \text{Tr}\left(\Phi_2^H \mathbf{D}_{\mathcal{F},k} \Phi_2 \mathbf{G}_{\mathcal{F},l}^r\right) \\
 \stackrel{(a_3)}{=} & \phi_2^H \left(\mathbf{D}_{\mathcal{F},k} \odot \mathbf{G}_{\mathcal{F},l}^r\right) \phi_2 \\
 \stackrel{(a_4)}{=} & \phi_2^H \Delta_{\mathcal{F},l,k} \phi_2, \quad l \in \mathcal{L}, \quad k \in \mathcal{K}, \quad (55)
 \end{aligned}$$

where (a₁) holds since (55) is a scalar and $\text{Tr}(\mathbf{A}\mathbf{B}) = \text{Tr}(\mathbf{B}\mathbf{A})$; (a₂) holds by defining $\mathbf{G}_{\mathcal{F},l}^r \triangleq \mathbf{g}_{\mathcal{F},l}^r \mathbf{g}_{\mathcal{F},l}^{rH}$ and $\mathbf{D}_{\mathcal{F},k} \triangleq d_{\mathcal{F},k}^H d_{\mathcal{F},k}$ for $\mathcal{F} \in \{s, m\}$; (a₃) can be derived in a similar manner as (49); and (a₄) holds by defining $\Delta_{\mathcal{F},l,k} \triangleq (\mathbf{D}_{\mathcal{F},k} \odot \mathbf{G}_{\mathcal{F},l}^r)$.

Then, we leverage the classical SDR technique [32], i.e., $\Omega = \bar{\phi}_2 \bar{\phi}_2^H$. By ignoring the rank-one constraint of Ω , we obtain a relaxed version of problem $\mathcal{P}6-E3$ as

$$\mathcal{P}6-E4 : \min_{\Omega} \text{Tr}(\Lambda\Omega) \quad (56)$$

$$\text{s.t. } \Omega_{(n,n)} = 1, \quad \text{for } \forall n \in \{N_2, N_2 + 1\}, \quad (56a)$$

$$\Omega \succeq 0, \quad (56b)$$

$$\text{Tr}(\tilde{\Delta}_{\mathcal{F},l,k}\Omega) = 0, \quad \text{for } \forall l \in \mathcal{L}, \quad \forall k \in \mathcal{K}. \quad (56c)$$

where

$$\tilde{\Delta}_{\mathcal{F},l,k} \triangleq \begin{bmatrix} \Delta_{\mathcal{F},l,k} & \mathbf{0}_{N_2 \times 1} \\ \mathbf{0}_{1 \times N_2} & 0 \end{bmatrix}. \quad (57)$$

Now, it can be observed that problem $\mathcal{P}6-E4$ has been transformed to a standard convex semidefinite program (SDP) and hence it can be optimally solved by existing convex optimization solvers such as CVX [33]. Then, we consider the rank one constraint, which means we need to recover the optimal $\bar{\phi}_2^*$ from the optimal Ω^* . By making the eigenvalue decomposition of Ω^* , we can get $\Omega^* = \mathbf{U}\Sigma\mathbf{U}^H$.

Next, we apply Gaussian randomization to obtain a large number of $\bar{\phi}_2 = \mathbf{U}\Sigma^{\frac{1}{2}}\mathbf{r}$, where $\mathbf{r} \sim \mathcal{CN}(0, \mathbf{I}_{M_2+1})$. From all $\bar{\phi}_2$ obtained with the different \mathbf{r} , we select the optimal $\bar{\phi}_2^*$ by maximizing the $\bar{\phi}_2\Lambda\bar{\phi}_2^H$. To satisfy the vector norm one constraint, we normalize the $\bar{\phi}_2^*$ as follows:

$$\phi_2^* = \exp\left(j \arg\left(\left[\frac{\bar{\phi}_2^*}{\bar{\phi}_2^*}_{(M_2+1)}\right]_{1:M_2}\right)\right). \quad (58)$$

The overall algorithm to optimize passive phase shifts θ_2 is summarized in Algorithm 2. In Step 1, the complexity

Algorithm 3 Modified Newton's Method to Update λ and η

Input: $\delta, \varepsilon, \varpi, \mathbf{v}, \mathbf{C}_s^*, \mathbf{C}_m^*, \lambda, \eta$

Output: updated $\lambda^{\text{upd}}, \eta^{\text{upd}}$

- 1: Initial $\mu = [\lambda, \eta], \psi(\mu)$ according to (61).
 - 2: Update to get μ^{upd} according to (62), where i satisfies (63).
 - 3: $\lambda^{\text{upd}} = \mu_{(1:L)}^{\text{upd}}, \eta^{\text{upd}} = \mu_{(L+1:2L)}^{\text{upd}}$.
-

of initialization which is dominated by calculating $\tilde{\Delta}$ is $\mathcal{O}(KLN_2^2 + L^2N_2^2M_2)$. In Step 2, the complexity of SDR that calculated by *First-Order Methods* is $\mathcal{O}\left(\frac{N_2^2\sqrt{\log N_2}}{\varepsilon_{SDR}^2}\right)$ [34], where ε_{SDR} is the target precision of SDR. Then, the complexity of Gaussian randomization from Step 3 to Step 6 is $\mathcal{O}(N_2^3 + N_{rand}N_2^2)$. Accordingly, the overall complexity of Algorithm 2 is $\mathcal{O}\left(N_2^2\left(KL + L^2M_2 + \frac{\sqrt{\log N_2}}{\varepsilon_{SDR}^2} + N_2 + N_{rand}\right)\right)$.

C. Update λ and η

In the last part of the BCD algorithm, we need to optimize λ and η with all variables $\beta^*, \mathbf{W}^*, \theta_1^*, \gamma^*, \mathbf{F}^*, \theta_2^*$ optimized and fixed. Special care needs to be taken that the problem $\mathcal{P}1-E2$ is convex programming with respect to parameters $\lambda_l \geq 0$ and $\eta_l \geq 0, l \in \mathcal{L}$. Accordingly, in what follows, λ and η are updated by using the modified Newton's method [35] until the convergence is achieved. Let $\mu^t = [\lambda^t, \eta^t]$ denote the parameter vector in the t th iteration. According to (21), we define

$$\psi_l^1(\mu) \triangleq -\varpi_l v_l + \eta_l(C_{s,l}^* + C_{m,l}^*), \quad l \in \mathcal{L}, \quad (59)$$

$$\psi_l^2(\mu) \triangleq -1 + \lambda_l(C_{s,l}^* + C_{m,l}^*), \quad l \in \mathcal{L}. \quad (60)$$

Let

$$\psi_l(\mu) = \psi_l^1(\mu), \quad \psi_{L+l}(\mu) = \psi_l^2(\mu), \quad l \in \mathcal{L}, \quad (61)$$

the optimal conditions $\psi_l^1(\mu) = \psi_l^2(\mu) = 0, l = 1, 2, \dots, L$ can be rewritten as $\psi(\mu) = \mathbf{0}$, which means we need to update μ^t until the convergence $\psi(\mu^{t+1}) = \mathbf{0}$ is recieved. If $\psi(\mu^t) = \mathbf{0}$, all variables $\beta^*, \mathbf{W}^*, \theta_1^*, \gamma^*, \mathbf{F}^*, \theta_2^*$ are the global solutions. Otherwise, we need to iterate μ^t by

$$\mu^{t+1} = \mu^t - \delta^{i^t} [\psi'(\mu^t)]^{-1} \psi(\mu^t), \quad (62)$$

where $\delta \in (0, 1), \varepsilon \in (0, 1), i$ denotes the smallest integer among $i \in \{0, 1, 2, \dots\}$ satisfying

$$\|\psi(\mu^{t+1})\| \leq (1 - \varepsilon\delta^i) \|\psi(\mu^t)\|, \quad (63)$$

and $\psi'(\mu^t)$ is the Jacobian matrix of $\psi(\mu^t)$, which can be easily obtained by calculating the partial derivatives as $\psi'(\mu^t) = \text{diag}(\mathbf{1}_{1 \times 2} \otimes (\mathbf{C}_s^* + \mathbf{C}_m^*))$. The λ and η are updated by iterations until $\psi(\mu^{t+1}) = \mathbf{0}$ is achieved. The whole procedures of update λ and η are summarized in Algorithm 3. The complexity of Algorithm 3 is dominated by calculating Jacobian matrix of $\psi(\mu)$. Since \mathbf{C}_s and \mathbf{C}_m are already known as the input, the complexity of Algorithm 3 can be ignored, because all steps are given by explicit mathematical expressions.

Algorithm 4 Overall BCD Algorithm to Solve Problem $\mathcal{P}0$

Input: $H, h_l^d, h_l^r, G_{\mathcal{F}}, g_{\mathcal{F},l}^r, g_{\mathcal{F},l}^d, d_{\mathcal{F},k}, \sigma_{\mathcal{F}}, P_{max}, T_{max}, \epsilon_1, \epsilon_2$
Output: $\alpha^*, \beta^*, \mathbf{W}^*, \theta_1^*, \gamma^*, \mathbf{F}^*, \theta_2^*$.

- 1: Initial $v_s^0, \beta^0, \mathbf{W}^0, \theta_1^0, \gamma^0, \mathbf{F}^0, \theta_2^0, \lambda^0, \eta^0, \delta, \varepsilon$ and $t = 0$.
- 2: **Repeat** (outer loop)
 - $t = t + 1$ and optimize v_s^t according to (12).
 - Repeat** (inner loop)
 - Optimize β^t to satisfy $\frac{\partial(f_{\mathcal{F},l})}{\partial\beta^t} = 0$.
 - Optimize \mathbf{F}^t according to (40).
 - Optimize \mathbf{W}^t according to *Algorithm 1*.
 - Optimize θ_1^t with the *SCA for the DL Phase Shift Optimization Algorithm* in [22].
 - Optimize γ^t to satisfy (38).
 - Optimize θ_2^t according to *Algorithm 2*.
 - Update λ^t and η^t according to *Algorithm 3*.
 - Until** Convergence $\|\psi(\mu^t)\| \leq \epsilon_1$ is achieved.
- Until** Convergence (64) is achieved or $t = T_{max}$.
- 3: $\alpha^* = [\frac{v_{s,1}^t}{v_1}, \dots, \frac{v_{s,L}^t}{v_L}]$, $\beta^* = \beta^t$, $\mathbf{W}^* = \mathbf{W}^t$, $\theta_1^* = \theta_1^t$, $\gamma^* = \gamma^t$, $\mathbf{F}^* = \mathbf{F}^t$, $\theta_2^* = \theta_2^t$.

D. Overall Algorithm to Solve Problem $\mathcal{P}0$

Up to now, we have completed the optimization for all blocks of the BCD algorithm. Based on the discussions above, we summarize and provide the whole steps of the BCD algorithm in the Algorithm 4. Firstly, in Step 1, all variables need to be initialized, where $\beta^0 \sim U(0, 1)$, $\alpha_l^0 \sim U(0, 1)$, $\gamma_l^0 \sim U(0, 1)$, $\theta_{1,n}^0$ and $\theta_{2,n}^0 \sim U(0, 2\pi)$. $\mathbf{W}^0 = \sqrt{P_{max}} \frac{\mathbf{W}}{\|\mathbf{W}\|_F}$, where \mathbf{W} is a $M_1 \times M_1$ complex matrix and real and imaginary parts of each element all distribute uniformly in $[-1, 1]$. \mathbf{F}^0 is the same distribution as \mathbf{W} . $\delta \sim U(0, 1)$, $\varepsilon \sim U(0, 1)$. Next, in Step 2, all variables are optimized block by block. And in each iteration, with $F_{obj}^t \triangleq \sum_{l=1}^L \varpi_l D_l(\alpha^t, \beta^t, \mathbf{W}^t, \theta_1^t, \gamma^t, \mathbf{F}^t, \theta_2^t)$, the number of iterations and the convergence in the following should be checked to determine whether the algorithm terminates:

$$\left| \frac{F_{obj}^t - F_{obj}^{t-1}}{F_{obj}^t} \right| \leq \epsilon_2. \quad (64)$$

It's worth noting that all of the proposed algorithms can guarantee to yield a monotonically decreasing objective function value of Problem $\mathcal{P}1$ in each step. Furthermore, the objective function value has a lower bound due to the power constraint. Accordingly, the BCD algorithm is guaranteed to converge to at least a locally optimal solution. The computational complexity of Algorithm 4 is mainly dependent on Step 2, whose complexities have been analyzed in the above subsections. If we fix the downlink energy transmission setting and pre-power the IoTs, the complexity of the overall algorithm can be reduced to $\mathcal{O}(t_{out} t_{in} (N_2^2 (KL + L^2 M_2 + \frac{\sqrt{\log N_2}}{\epsilon_{SDR}^2} + N_2 + N_{rand})))$, where t_{out} and t_{in} are the number of outer iterations and inner iterations, respectively.

V. TRADE-OFF BETWEEN DOPPLER MITIGATION AND LATENCY MINIMIZATION

In Section III and IV, we have designed and optimized the downlink and uplink settings carefully to minimize the upload latency of the proposed double IRSs aided IoT system. However, in HSR scenes, the increased Doppler shift due to the high speed movement of the train can make a significant impact on the performance of the communication system, causing the IoT system to fail to achieve the expected performance. Larger Doppler spread results in shorter channel coherence times, which can reduce the effective achievable rate of the system by the pilot overhead, resulting in greater information upload latency. Therefore, in this section, the feasibility of mitigating the Doppler spread stemming from the movement of train is also investigated by utilizing the IRS2 based on the optimized uplink setting. Before presenting the specific Doppler mitigation algorithm, the well-known Doppler shift phenomenon is revisited in the proposed system. The high-speed train travels through the IoTs coverage area with a constant speed v m/s. For the direct link, the Doppler spread can be easily get by

$$f_{d,d,t} = \max\left(\frac{v_{speed} \cos \varphi_{d,t}}{\lambda_{\mathcal{F}}}\right) = \frac{v_{speed} \cos \varphi_{d,t}}{\lambda_m}, \quad (65)$$

where λ_m and $\varphi_{d,t}$ are the wavelength of mmWave and horizontal angle of arrival of the direct link in t th time slot, respectively. For the cascaded link, the Doppler shift phenomenon is caused by the motion of the train leading to a change in the phase of the received signals per unit time, which results in the signals frequency change. Since the train and IRS2 are relatively fixed, only the IoTs to the IRS2 link generates phase differences. Without considering the near-field effect, the phase difference per unit time of the n th passive element in t th time slot is

$$\Delta\phi_{n,t} = \frac{2\pi v_{speed} \Delta t \cos \varphi_{c,t}}{\lambda_m} + (\theta_{2,n,t}^* - \theta_{2,n,t-1}^*), \quad (66)$$

where Δt and $\varphi_{c,t}$ are one slot time and horizontal angle of arrival of the cascaded link, respectively. Then, the Doppler spread is the maximum difference in instantaneous frequency over all significant propagation links [36]. The Doppler spread of the cascaded link is

$$\begin{aligned} f_{d,c,t} &= \max_{n_1, n_2} \left| \frac{\Delta\phi_{n_1,t} - \Delta\phi_{n_2,t}}{2\pi\Delta t} \right| \\ &= \max_{n_1, n_2} \left| \frac{(\theta_{2,n_1,t}^* - \theta_{2,n_1,t-1}^*) - (\theta_{2,n_2,t}^* - \theta_{2,n_2,t-1}^*)}{2\pi\Delta t} \right|, \\ & n_1, n_2 \in \mathcal{N}_2. \end{aligned} \quad (67)$$

Note that n_1, n_2 refers to the different element in the IRS2. Mitigating Doppler spread by IRS has been proven to be feasible [37]. It is essential to mitigate the Doppler spread by reducing the phase difference between different paths. Although we cannot completely eliminate the Doppler spread due to the existence of the direct link [37], we can still reduce its impact on the whole system by mitigating it. As the formula (67) shows, we can optimize the phase shifts of passive elements on the IRS2 to reduce the phase difference and thus the Doppler spread. But simply adjusting the passive

Algorithm 5 Heuristic Algorithm for Doppler Mitigation

Input: $\varphi_{d,t}, \varphi_{c,t}, v_{speed}, \theta_{2,t}^*, \theta_{2,t-1}^*, \lambda_m, N_2, po, T,$

Output: $\theta_{2,t}^{DM}$.

- 1: Initial $t = 1, \theta_{2,t}^{DM} = \theta_{2,t}^*$.
 - 2: **Repeat**
 - 3: $t = t + 1$ and calculate the Doppler spread of the direct link $f_{d,d,t}$ according to (65).
 for $n = 1 : N_2$
 - 4: Calculate $\Delta\phi_{n,t}$ according to (66).
 end
 - 5: Sort $\Delta\phi_{n,t}$ in descending order and update subscript index.
 - 6: Find m , which satisfies $\frac{\Delta\phi_{m,t} - \Delta\phi_{N_2,t}}{2\pi\Delta t} \geq f_{d,d,t}$ and $\frac{\Delta\phi_{m+1,t} - \Delta\phi_{N_2,t}}{2\pi\Delta t} \leq f_{d,d,t}$.
 for $n = 1 : m$
 - 7: Calculate $\theta_{2,n,t}^{DM} = \theta_{2,n+1,t}^* + \theta_{2,n,t-1}^* - \theta_{2,n+1,t-1}^*$.
 - 8: Calculate $OB_t^{DM} = \sum_{l=1}^L \varpi_l D_l(\theta_{2,t}^{DM})$ and $OB_t^* = \sum_{l=1}^L \varpi_l D_l(\theta_{2,t}^*)$.
 - 9: **if** $(OB_t^{DM} < OB_t^* \text{ or } OB_t^{DM} < OB_{t-1}^*)$, **break**;
 end
 - 10: **Until** $t = T$.
-

elements will destroy the already aligned phase shifts. Adjusting the phase shifts to minimize the Doppler spread will improve the coherence time of the channel but increase the information upload latency, while adjusting the phase shifts to minimize the information upload latency will result in an increase in the Doppler spread, which will also increase the information upload latency. There is obviously a trade-off between maximization of the data rate and Doppler mitigation and how to find it is a very tricky problem. Consequently, we proposed a low complexity heuristic algorithm which is presented in Algorithm 5, where po denotes the pilot overhead and T denotes the total time slots.

Note that in Step 6, the boundary m of passive elements is found since the Doppler spread of the direct link cannot be eliminated. The Doppler spread of the cascaded link only needs to be reduced to the level of the direct link to prevent excessive performance loss. In Step 7, we adjust the passive elements one by one to reduce phase differences. According to (67), to mitigate Doppler spread, we make $\Delta\phi_{n,t} - \Delta\phi_{N_2,t} = \Delta\phi_{n+1,t} - \Delta\phi_{N_2,t}$, which means the adjusted phase shift $\theta_{2,n,t}^{DM}$ should be $\theta_{2,n,t}^{DM} = \theta_{2,n+1,t}^* + \theta_{2,n,t-1}^* - \theta_{2,n+1,t-1}^*$. Then, in Step 8 and 9, the object functions are calculated to compare whether the performance degrades. If so, the algorithm stops.

The complexity of the heuristic algorithm is dominated by calculating OB_t^{DM} and OB_t^* , whose complexities are on the order of $\mathcal{O}(TLM_2^2)$.

VI. SIMULATIONS AND RESULTS

In this section, we provide numerical results to examine the performance of our proposed algorithms. The benefits of deploying the double IRSs in the HSR IoT system are evaluated. We consider a HSR IoT system aided by double IRSs in single-cell for $L = 3$ devices. As for the channel

model, both the small scale fading and the large scale path loss are considered. The small scale fading follows the complex Gaussian distribution associated with zero mean and unit variance, while the path loss is given by $\rho = \rho_0 \left(\frac{d}{d_0}\right)^{-\alpha}$, where $\rho_0 = -20$ dB is the large-scale fading factor at the reference distance of $d_0 = 1$ m [38]. Then, we set $\alpha_{ref} = 2.2$ and $\alpha_{dir} = 3.5$, where α_{ref} denotes the path loss exponent of reflecting links and α_{dir} denotes that of direct links, respectively [16, 38]. The distances from BS to IRS1 d_H , from BS to IoTD d_{hd} , from IRS1 to IoTD d_{hr} , from IoTD to IRS2 d_{gr} , from IoTD to MCR d_{gd} , from IRS2 to MCR d_G , from IRS2 to user d_d are set as 10 m, 10 m, 5 m, 9 m, 10 m, 2 m and 7m, respectively. To satisfy the zero forcing constraint in (8), we set the zenith of departure and zenith of arrival of the light of sight (LoS) path for all users as $\frac{3\pi}{4}$ and $\frac{\pi}{4}$, respectively. It's worth noting that the AoAs and AoDs of all users are still random. This is reasonable since the geometric distribution of the passengers in the train is characterized by linearity. With the assumption, the passive beam is easy to optimize to block users who are in the given directions. For all channels, the small-scale fading is assumed to be Rician fading. In specific, the small-scale channel can be modeled as

$$\tilde{\mathbf{H}} = \sqrt{\frac{\kappa}{\kappa + 1}} \tilde{\mathbf{H}}^{\text{LoS}} + \sqrt{\frac{1}{\kappa + 1}} \tilde{\mathbf{H}}^{\text{NLoS}}, \quad (68)$$

where κ is the Rician factor, $\tilde{\mathbf{H}}^{\text{LoS}}$ is the deterministic line of sight (LoS), and $\tilde{\mathbf{H}}^{\text{NLoS}}$ is the non-LoS (NLoS) component which is the Rayleigh fading. The LoS component $\tilde{\mathbf{H}}^{\text{LoS}}$ is generated by typical geometric channel model, which is given by $\tilde{\mathbf{H}}^{\text{LoS}} = \mathbf{a}_{xy}(\theta^{AoA}, \theta^{ZoA}) \mathbf{a}_{xy}^H(\theta^{AoD}, \theta^{ZoD})$, where \mathbf{a}_{xy} is defined as

$$\mathbf{a}_{xy}(\theta_1, \theta_2) = \mathbf{a}_x(\theta_1, \theta_2) \otimes \mathbf{a}_y(\theta_1, \theta_2), \quad (69)$$

where \mathbf{a}_x and \mathbf{a}_y are antenna array response vectors, they can be written as

$$\mathbf{a}_x(\theta_1, \theta_2) = \left[1, e^{j\frac{2\pi d_x}{\lambda} \sin \theta_1 \cos \theta_2}, \dots, e^{j\frac{2\pi d_x}{\lambda} (M_x - 1) \sin \theta_1 \cos \theta_2} \right]^T, \quad (70)$$

$$\mathbf{a}_y(\theta_1, \theta_2) = \left[1, e^{j\frac{2\pi d_y}{\lambda} \sin \theta_1 \sin \theta_2}, \dots, e^{j\frac{2\pi d_y}{\lambda} (M_y - 1) \sin \theta_1 \sin \theta_2} \right]^T, \quad (71)$$

where d_x and d_y are the distance between elements along the X-axis and Y-axis, respectively, and M_x, M_y are the number of passive elements along the X-axis and Y-axis, respectively. The NLoS component $\tilde{\mathbf{H}}^{\text{NLoS}}$ follows the complex-valued Gaussian distribution that $\tilde{\mathbf{H}}^{\text{NLoS}} \sim \mathcal{CN}(0, \mathbf{I})$.

Next, the volume of uploaded task v_l is set randomly and obeys uniform distribution, which means $v_l \sim U(1000, 2000)(kb)$. The weights of all IoTDs are also obey uniform distribution. To facilitate analysis, the volumes of all tasks and weights are fixed in the following simulations. The other default settings of system-related parameters are summarised as follows: Antenna numbers $M_1 / M_2 = 25 / 9$. Passive element numbers $N_1 / N_2 = 100 / 100$. Number of users and IoTDs K and L are all 3. Carrier frequency $f_s / f_m = 3.5 / 28$ GHz [39]. Bandwidths $B_s / B_m = 10 / 80$ MHz

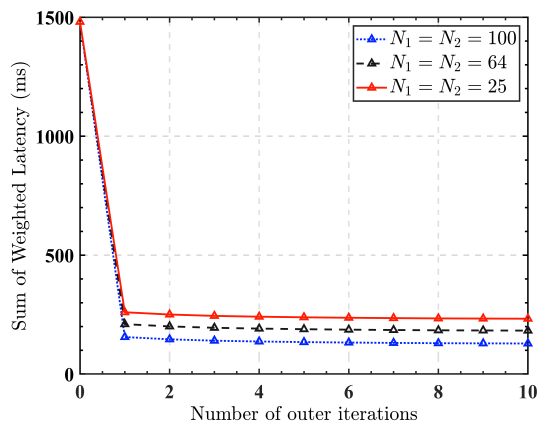


Fig. 3. Outer iterations convergence behavior of the BCD Algorithm.

TABLE I
SIMULATION PARAMETERS

Antenna numbers M_1 / M_2	25 / 9
Passive element numbers N_1 / N_2	100 / 100
Number of users K	3
Number of IoTDs L	3
Carrier frequency f_s / f_m	3.5 GHz / 28 GHz [39]
Bandwidths B_s / B_m	10 / 80 MHz [40]
Rician factor κ	6 [41]
Transmission power P_{\max}	10 W
Power spectral density of the noise	-174 dBm [40]
Energy transmission efficiency ξ	0.8

[40]. Rician factor $\kappa = 6$ [41]. Transmission power $P_{\max} = 10$ W. Power spectral density of the noise = -174 dBm [40].

First, we simulate the convergence behavior of our proposed BCD Algorithm averaged over 100 independent channel realizations and the result is shown in Fig. 2 and Fig. 3. It’s observed that our proposed BCD algorithm converges monotonically, which is in line with our analysis in Section IV. In Fig. 2, the outer loop can decrease quickly in two iterations. The sum of weighted latency drops by 90% in the first iteration, which shows that we can obtain most of the latency improvement in the first two iterations and our proposed algorithm has an extremely low complexity. What’s more, the convergence behaviors show similar trends under different settings of double IRSs phase shift number, i.e. $N_1 = N_2 = 25, 64,$ and 100 . As the number of elements increases, the latency decreases. The reason is obvious that the energy efficiency of the transmission and the channel capacity are enhanced. Although the BCD algorithm may require more than 10 outer iterations for full convergence, the latter iterations have little performance improvement, and in a practical scenario, we can set the maximum number of outer iterations to 2. In Fig. 3, the inner loop behaviors are investigated. From Fig. 3(a), the latency can almost converge in three inner iterations of the first outer iteration. And in Fig. 3(b), the latency can obtain little improvement in three inner iterations of the second outer iteration. A similar conclusion can be drawn from Fig. 3(c).

Next, we compare the BCD Algorithm with the following benchmark schemes:

1) **Random Energy Beams \mathbf{W}** : The energy beams \mathbf{W} in

downlink energy transmit setting is fixed in each iteration. Both the real and imaginary parts of the energy beams matrix \mathbf{W} follow independent uniform distribution in $(0, 1)$. Then, it is initialized by $\|\mathbf{W}\|_F^2 = 10$. The numbers of passive elements of both IRSs are all fixed at 100.

2) **No IRS1/IRS2**: The system without one of double IRSs still can complete the transmission task, though there will be some performance loss. The number of passive elements of the other one IRS is fixed at 100.

3) **Random Phase Shifts with IRS1/IRS2**: The phase shifts of one IRS are generated randomly following uniform distribution in $[0, 2\pi)$, while the phase shifts of the other one are optimized. Similarly, the number of passive elements of the other IRS is fixed at 100. In Fig. 4, we compare the latency by all schemes versus the transmit power P_t of the BS. Specifically, the latency reductions of all schemes become quite pronounced upon increasing transmit power. This is obvious because the IoTDs can harvest more energy from the BS for information transmission. And when the random energy beams \mathbf{W} is fixed without optimization, there is a significant drop in latency performance, especially at low transmitting power. As the transmit power rises, the sum weighted latency gap between the RandomEnergy Beams and the Optimal Phase decreases, so that the optimization of \mathbf{W} has a greater impact on the system when energy is scarce.

The optimized phase shifts of double IRSs can efficiently decrease the latency of information upload than that of random phase shifts in benchmarks. Additionally, our proposed algorithm performs better in low transmit power condition, which means the double IRSs deployment scheme is more suitable for energy-scarce scenarios. This is mainly because when transmit power is too low, the performance bottleneck of the whole system is the energy received by all IoTDs.

Fig. 5 presents the influence of performance latency for the five benchmark schemes and the proposed BCD algorithm versus the number of passive elements. Firstly, similar to what we learned from Fig. 4, our proposed BCD algorithm obviously outperforms other benchmarks. The latency of all schemes decreases with the number of passive elements. The sum of weighted latency can decrease to 130 ms. Secondly, as we can see from curves of both IRSs, the performance gap between the benchmarks “noIRS1/IRS2” and “RandomPhase of IRS1/IRS2” becomes higher upon increasing the number of reflecting elements. It implies that the double IRSs are capable of assisting the energy and information transmission. And with careful phase shifts optimized by the proposed algorithm, the performance can be further improved. Thirdly, under the default system setting, deploying the IRS at the IoTd side to assist the energy transmission performs better than that at the MCR side to assist the information transmission. We will discuss how to allocate the elements of IRSs in the next.

In Fig. 6, we study the impact of allocating passive elements of double IRSs on the system latency. The curve changes versus the number of passive elements on IRS1, with the total number of elements is fixed at 200, which means $N_1 + N_2 = 200$. It’s obvious that with the transmit power increases, the summation of weighted latency decreases. Furthermore, as a resource, a certain number of passive

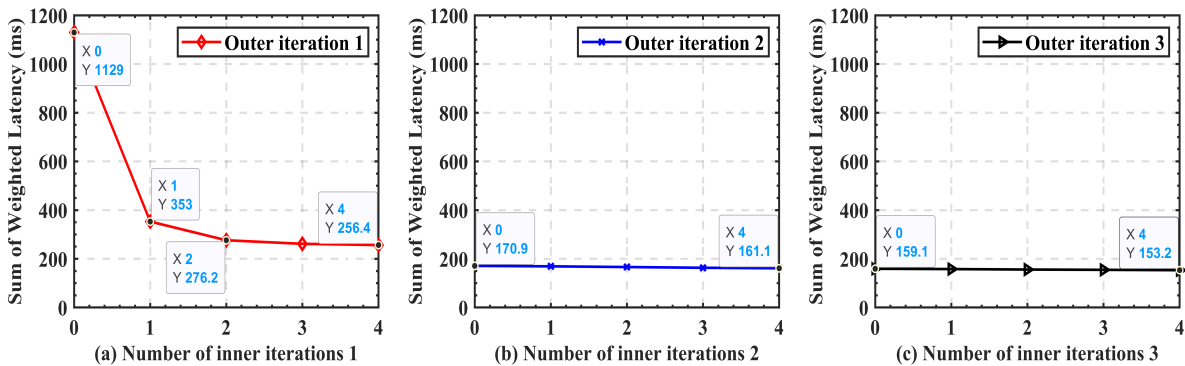


Fig. 4. Sum of weighted latency versus the number of inner iterations

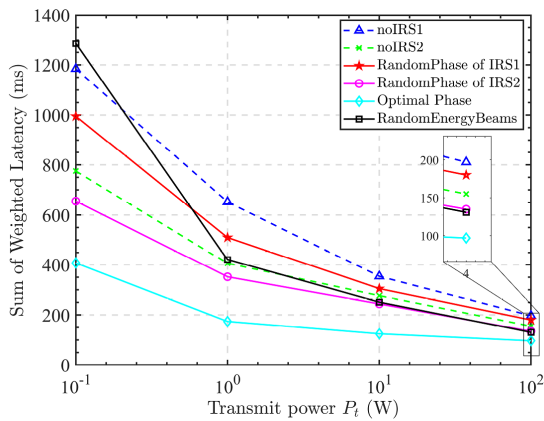
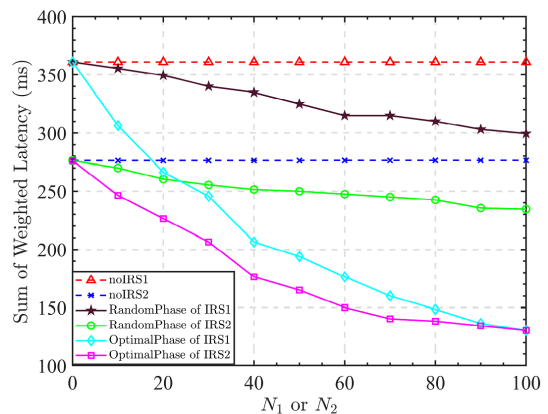
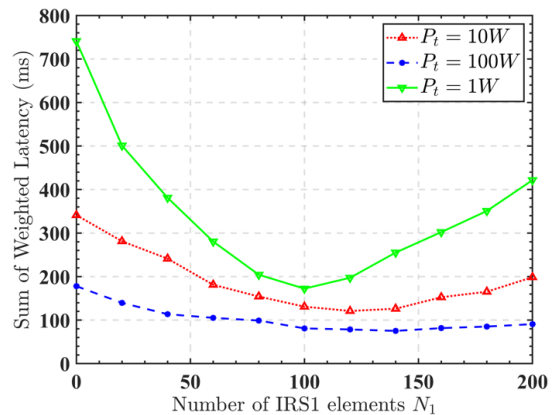

 Fig. 5. Sum of weighted latency versus the transmit power P_t .


Fig. 6. Sum of weighted latency versus the number of passive elements.

elements should be appropriately allocated for maximization of the harvest energy and channel capacity to minimize the latency. Accordingly, there exists an inherent trade-off in the N_1/N_2 allocation among the double IRSs. Note that the elements allocation is more significant in low transmitting power case. As the transmit power increases, the effect of elements allocation becomes weaker and weaker. Although the increase in power can lead to a decrease in latency, it is not linear. This is a typical phenomenon of diminishing marginal benefits. The optimal elements assignment reduces the latency by approximately 50% compared to assigning the elements all to one IRS. So N_1 and N_2 require more careful design especially when energy is scarce. Furthermore, when energy transmission power $P_t = 1W$, the latency of the scheme can be minimized at approximately $N_1 = 100$, $N_2 = 100$. With the increase of P_t , the trade-off point moves to the right. The main reason is that when energy transmission is low, there is a performance bottleneck due to received energy by all IoTs. Even though the IRS2 improves the channel conditions, the lack of transmission energy leads to performance degradation. In the case of lower transmitting power, more elements that deployed on IRS1 can help achieve the desirable latency. And the specific elements of IRSs allocation scheme needs to be determined according to the specific environment.

In the next, we firstly define the total information leakages


 Fig. 7. Sum of weighted latency versus the number of passive elements N_1 with $N_1 + N_2 = 200$. (b) Sum of weighted latency versus the number of passive elements.

to passengers as follows:

$$\zeta = \sum_{k=1}^K \sum_{l=1}^L \sum_{\mathcal{F}} |d_{\mathcal{F},k} \Phi_2 g_{\mathcal{F},l}^r|^2, \quad (72)$$

As shown in Fig. 7, we investigate the ζ against the number of passive elements of IRS2. From the figure, with the increase of the number of passive elements, the leakage ζ with

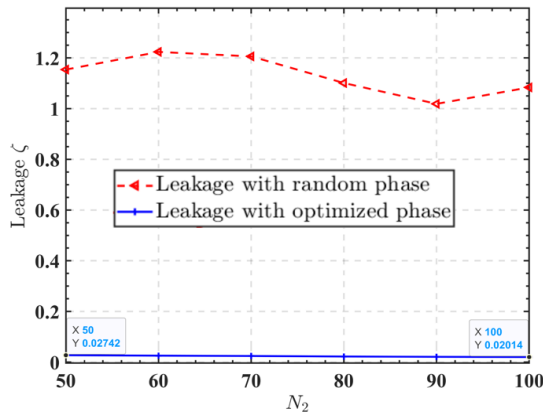


Fig. 8. Sum of weighted latency versus the number of passive elements.

optimized phase shifts does not change significantly and never drops to 0 though the constraint (56c) is introduced. The main reason is that the passive beamforming with finely designed of IRS2 can shield the LoS path to the users, but some of other NLoS paths will still leak. Also, we relaxed the rank one constraint when optimizing the phase shifts in Algorithm 2, which means the constraint (56c) has been broken when eigenvalue decomposition and Gaussian randomization are applied. The total leakages are reduced by approximately 97.5% compared to the pre-optimization period. With the deployment of the IRS2, the total leakages to all users can be reduced to an extremely low level. Although the improvement is slight, the system exhibits a decrease in leakage as the number of passive elements increases. This is because with more elements, the narrower passive beams are generated and the leakage to NLoS paths decreases. It is worth noting that a sufficient number of passive elements need to be deployed to ensure that the passive beam can be finely designed, otherwise problem $\mathcal{P6-E4}$ will lead to no solution due to constraint (56c). In conclusion, the IoT communication system aided by IRSs allows for covert communication thus ensuring the security of train communication from the perspective of physical layer.

Then, to validate the effectiveness of our proposed Doppler mitigation (DM) algorithm, we investigate the sum of weighted latency against the position of train when train travels through the accident-prone area where IoTDs and IRS are deployed. We consider a simulation setting that the train travels from far away from IoTDs to close to IoTDs and then away again. The train is 20 m away from IoTD at the farthest and only 1 m at the closest. And the pilot overhead (p_o) is fixed at 6000. From the Fig. 8, as the train travels, the sum weighted latency of all curves is constantly changing. What's more, the sum weighted latency of the system is directly related to the distance between the IoTDs and the train. It is higher when the train is further away from the IOTDs. Due to the influence of channel coherence time, the faster the train's speed, the worse the system performance. More importantly, our proposed DM algorithm can greatly improve the performance of communication system than no DM algorithm and thus reduce the sum weighted latency. The performance improvement of the proposed algorithm is more significant when the train's speed

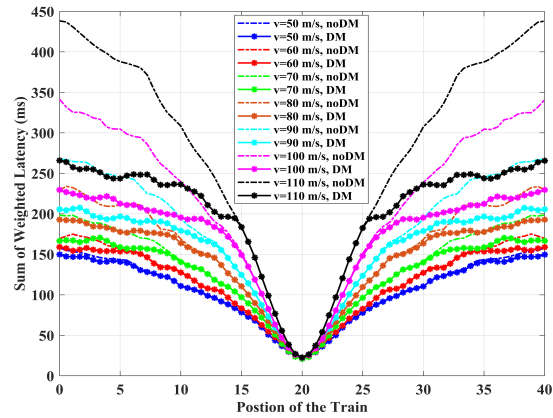


Fig. 9. Sum of weighted latency versus train's position with different speed.

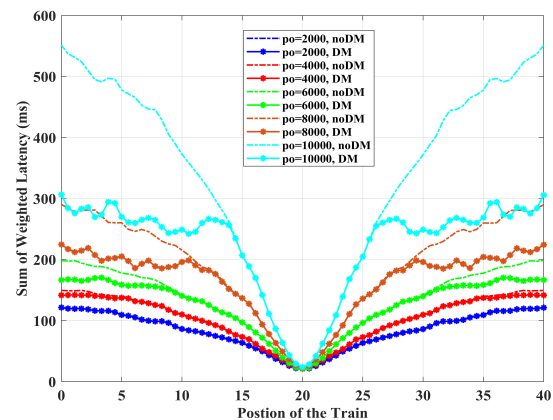


Fig. 10. Sum of weighted latency versus the position of train with different pilot overhead.

is faster. At the farthest distances, the sum weighted latency can be reduced by 40% when train's speed $v=110$ m/s while there is little improvement when $v=50$ m/s. It's worth noting that as the train's speed increases, the applicable distance of the DM algorithm becomes longer and longer, from $0\sim 4$ m at $v=50$ m/s to $0\sim 15$ m at $v=110$ m/s. This is obvious because as the distance gets farther and the speed gets faster, the greater the Doppler spread, and the greater the Doppler mitigation by the proposed algorithm. Then, the train's speed is fixed at $v=70$ m/s (≈ 250 km/h). The simulation result is shown in Fig. 9. Similar to that in Fig. 8, when p_o is higher, the performance improvement is more significant.

VII. CONCLUSION

In this paper, we have proposed a framework of HSR IoT communication systems by deploying double IRSs at both track side and MCR side. Our simulation results verified that by carefully designing the phase shifts of double IRSs block by block, the summation information upload latency can be minimized by more than 90%. Furthermore, the deployment of passive elements on multi IRSs should be carefully designed to guarantee the optimal performance according to the specific travel environment, especially when energy is scarce. In our future work, we will consider generating the optimal historical

hybrid beams, including energy beams \mathbf{W} , passive beams θ_1, θ_2 as the output of the deep neural network to learn the state characteristics of train for CSI-free online beam optimization. deploying active IRSs in HSR scenario. The active elements design and resource optimization of WPCN in the HSR IoT scenario need to be thoroughly investigated from the perspective of energy consumption.

REFERENCES

- [1] A. Eduard, D. Urazayev, A. Sabyrbek, D. Orel, and D. Zorbas, "Ad-hoc train-arrival notification system for railway safety in remote areas," *Internet of Things*, vol. 25, p. 101062, 2024.
- [2] A. Padovano, F. Longo, L. Manca, and R. Grugni, "Improving safety management in railway stations through a simulation-based digital twin approach," *Computers & Industrial Engineering*, vol. 187, p. 109839, 2024.
- [3] S. Janani, S. Vijayaram, and R. Vijayganes, "Iot-saferails: Revolutionizing railway collision avoidance technology," in *2024 International Conference on Inventive Computation Technologies (ICICT)*. IEEE, 2024, pp. 1666–1673.
- [4] M. Palanivelan, E. Karthick, G. Gnanaprakash, et al., "Intelligent load monitoring and control in railway wagons using iot," in *2024 International Conference on Computing and Data Science (ICCDs)*. IEEE, 2024, pp. 1–6.
- [5] M. M. R. Nayan, S. A. Sufi, A. K. Abedin, R. Ahamed, and M. F. Hossain, "An IoT based real-time railway fishplate monitoring system for early warning," in *2020 11th International Conference on Electrical and Computer Engineering (ICECE)*, 2020, pp. 310–313.
- [6] B. A. Khivsara, P. Gawande, M. Dhanwate, K. Sonawane, and T. Chaudhari, "IOT based railway disaster management system," in *2018 Second International Conference on Computing Methodologies and Communication (ICCMC)*, 2018, pp. 680–685.
- [7] L. Yan, X. Fang, and Y. Fang, "Control and data signaling decoupled architecture for railway wireless networks," *IEEE Wireless Communications*, vol. 22, no. 1, pp. 103–111, 2015.
- [8] B. Ai, K. Guan, M. Rupp, T. Kurner, X. Cheng, X.-F. Yin, Q. Wang, G.-Y. Ma, Y. Li, L. Xiong, and J.-W. Ding, "Future railway services-oriented mobile communications network," *IEEE Communications Magazine*, vol. 53, no. 10, pp. 78–85, 2015.
- [9] G. Zhong, K. Xiong, Z. Zhong, and B. Ai, "Internet of things for high-speed railways," *Intelligent and Converged Networks*, vol. 2, no. 2, pp. 115–132, 2021.
- [10] P. Ramezani and A. Jamalipour, "Optimal resource allocation in backscatter assisted wpcn with practical energy harvesting model," *IEEE Transactions on Vehicular Technology*, vol. 68, no. 12, pp. 12406–12410, 2019.
- [11] H. Tang, Q. Wu, W. Chen, J. Wang, and B. Li, "Mitigating the doubly near-far effect in uav-enabled wpcn," *IEEE Transactions on Vehicular Technology*, vol. 70, no. 8, pp. 8349–8354, 2021.
- [12] J. Yi, S. Kim, J. Kim, and S. Choi, "Supremo: Cloud-assisted low-latency super-resolution in mobile devices," *IEEE Transactions on Mobile Computing*, vol. 21, no. 5, pp. 1847–1860, 2022.
- [13] Q. Wu and R. Zhang, "Towards smart and reconfigurable environment: Intelligent reflecting surface aided wireless network," *IEEE Communications Magazine*, vol. 58, no. 1, pp. 106–112, 2020.
- [14] J. Zhang, H. Liu, Q. Wu, Y. Jin, Y. Chen, B. Ai, S. Jin, and T. J. Cui, "RIS-aided next-generation high-speed train communications: Challenges, solutions, and future directions," *IEEE Wireless Communications*, vol. 28, no. 6, pp. 145–151, 2021.
- [15] J. Xu and B. Ai, "When mmwave high-speed railway networks meet reconfigurable intelligent surface: A deep reinforcement learning method," *IEEE Wireless Communications Letters*, vol. 11, no. 3, pp. 533–537, 2022.
- [16] C. Pan, H. Ren, K. Wang, W. Xu, and L. Hanzo, "Multicell MIMO communications relying on intelligent reflecting surfaces," *IEEE Transactions on Wireless Communications*, vol. PP, no. 99, 2020.
- [17] C. Xu, J. An, T. Bai, S. Sugiura, R. G. Maunder, Z. Wang, L.-L. Yang, and L. Hanzo, "Channel estimation for reconfigurable intelligent surface assisted high-mobility wireless systems," *IEEE Transactions on Vehicular Technology*, vol. 72, no. 1, pp. 718–734, 2023.
- [18] Y. Wang, G. Wang, R. Xu, R. He, B. Ai, and H. Xiao, "Joint channel estimation and data detection for intelligent transparent surface (its) aided wireless communications on railways," in *2021 13th International Conference on Wireless Communications and Signal Processing (WCSP)*, 2021, pp. 1–5.
- [19] Z. Ma, Y. Wu, M. Xiao, G. Liu, and Z. Zhang, "Interference suppression for railway wireless communication systems: A reconfigurable intelligent surface approach," *IEEE Transactions on Vehicular Technology*, vol. 70, no. 11, pp. 11593–11603, 2021.
- [20] L. Zhou, K.-H. Yeh, G. Hancke, Z. Liu, and C. Su, "Security and privacy for the industrial internet of things: An overview of approaches to safeguarding endpoints," *IEEE Signal Processing Magazine*, vol. 35, no. 5, pp. 76–87, 2018.
- [21] C. Feng, H.-M. Wang, and H. V. Poor, "Reliable and secure short-packet communications," *IEEE Transactions on Wireless Communications*, vol. 21, no. 3, pp. 1913–1926, 2022.
- [22] X. Li, C. Zhang, C. He, G. Chen, and J. A. Chambers, "Sum-rate maximization in IRS-assisted wireless power communication networks," *IEEE Internet of Things Journal*, vol. PP, no. 99, 2021.
- [23] Y. Zhao, J. Zhang, and B. Ai, "Applications of reconfigurable intelligent surface in smart high-speed railway communications," *ZTE Communications*, vol. 27, no. 4, 2021.
- [24] H. Liu, J. Zhang, Q. Wu, Y. Jin, Y. Chen, and B. Ai, "RIS-aided next-generation high-speed train communications: Challenges, solutions, and future directions," 2021. [Online]. Available: <https://arxiv.org/abs/2103.09484>
- [25] Q. Wu, S. Zhang, B. Zheng, C. You, and R. Zhang, "Intelligent reflecting surface-aided wireless communications: A tutorial," *IEEE Transactions on Communications*, vol. 69, no. 5, pp. 3313–3351, 2021.
- [26] H. Ju and R. Zhang, "Throughput maximization in wireless powered communication networks," *IEEE Transactions on Wireless Communications*, vol. 13, no. 1, pp. 418–428, 2014.
- [27] C. Qiu, Q. Wu, M. Hua, X. Guan, and Y. Wu, "Achieving multi-beam gain in intelligent reflecting surface assisted wireless energy transfer," *IEEE Transactions on Vehicular Technology*, vol. 72, no. 3, pp. 4052–4057, 2023.
- [28] S. Zeng, H. Zhang, B. Di, Y. Tan, Z. Han, H. V. Poor, and L. Song, "Reconfigurable intelligent surfaces in 6g: Reflective, transmissive, or both?" *IEEE Communications Letters*, vol. 25, no. 6, pp. 2063–2067, 2021.
- [29] Q. Shi, M. Razaviyayn, Z.-Q. Luo, and C. He, "An iteratively weighted MMSE approach to distributed sum-utility maximization for a mimo interfering broadcast channel," *IEEE Transactions on Signal Processing*, vol. 59, no. 9, pp. 4331–4340, 2011.
- [30] "DC Programming: The optimization method you never knew you had to know," 2012, MIT OpenCourseWare. [Online]. Available: https://ocw.mit.edu/courses/sloan-school-of-management/15-097-prediction-machine-learning-and-statistics-spring-2012/projects/MIT15_097S12_proj5.pdf
- [31] X. Zhang, *Matrix analysis and applications*. Cambridge University Press, 2017.
- [32] Z.-q. Luo, W.-k. Ma, A. M.-c. So, Y. Ye, and S. Zhang, "Semidefinite relaxation of quadratic optimization problems," *IEEE Signal Processing Magazine*, vol. 27, no. 3, pp. 20–34, 2010.
- [33] M. Grant and S. Boyd, "CVX: Matlab software for disciplined convex programming," 2014.
- [34] I. Waldspurger, A. d'Aspremont, and S. Mallat, "Phase recovery, maxcut and complex semidefinite programming," *Mathematical Programming*, vol. 149, pp. 47–81, 2015.
- [35] Y. Jong, "An efficient global optimization algorithm for nonlinear sum-of-ratios problem," *Optimization Online*, pp. 1–21, 2012.
- [36] R. G. Gallager et al., *Principles of digital communication*. Cambridge University Press Cambridge, UK, 2008, vol. 1.
- [37] E. Basar, "Reconfigurable intelligent surfaces for doppler effect and multipath fading mitigation," *frontiers in Communications and Networks*, vol. 2, p. 672857, 2021.
- [38] C. Hu, L. Dai, S. Han, and X. Wang, "Two-timescale channel estimation for reconfigurable intelligent surface aided wireless communications," *IEEE Transactions on Communications*, pp. 1–1, 2021.
- [39] A. Ali, N. González-Prelcic, and R. W. Heath, "Millimeter wave beam-selection using out-of-band spatial information," *IEEE Transactions on Wireless Communications*, vol. 17, no. 2, pp. 1038–1052, 2018.
- [40] T. Li, Y. Xu, H. Tong, and K. Pang, "Low-band information and historical data aided non-uniform millimeter wave beam selection algorithm in 5G-R high-speed railway communication scene," *IEEE Transactions on Vehicular Technology*, vol. 71, no. 3, pp. 2809–2823, 2022.
- [41] T. Li, H. Tong, Y. Xu, X. Su, and G. Qiao, "Double irss aided massive mimo channel estimation and spectrum efficiency maximization for high-speed railway communications," *IEEE Transactions on Vehicular Technology*, vol. 71, no. 8, pp. 8630–8645, 2022.